TEMPORAL SCALES OF TROPOSPHERIC CO_2, PRECIPITATION, AND ECOSYSTEM RESPONSES IN THE CENTRAL U.S.

BY

Ferdouz Vuilliomenet Cochran

Submitted to the graduate degree program in Geography and the Graduate Faculty of the University of Kansas in partial fulfillment of the requirements for the degree of Master of Arts

---

Dr. Nathaniel A. Brunsell
Chairperson

Dr. David B. Mechem

Dr. William C. Johnson

Date Defended: July 29, 2011

The Thesis Committee for Ferdouz Vuilliomenet Cochran
certifies that this is the approved version of the following thesis:

TEMPORAL SCALES OF TROPOSPHERIC CO_2, PRECIPITATION,

AND ECOSYSTEM RESPONSES IN THE CENTRAL U.S.

Dr. Nathaniel A. Brunsell
Chairperson

Date Approved: July 29, 2011

ACKNOWLEDGMENTS

This research was funded in part by the National Science Foundation EPSCoR KAN0061396.KAN006263. Additional funding for F.V. Cochran was provided through the IGERT C-CHANGE NSF080152 program. Thank you to the AIRS Project, NASA/JPL-Caltech, for development of the mid-tropospheric CO_2 product; the NOAA Climate Prediction Center/OAR/ESRL PSD, Boulder, Colorado, USA (http://www.esrl.noaa.gov/psd/) for the US Unified Precipitation data product; and the USGS Earth Resources Observation and Science and NASA Land Processes Distributed Active Archive Center for the MODIS NDVI data product. Special appreciation to T. Buck and A. Quick for assistance with processing of the eddy covariance data; the KU Biometeorology Lab, C-CHANGE Fellows, and CReSIS faculty, staff, and students for inspiration and moral support; D. Mechem for edits and honest discussion; and N. Brunsell for knowledge, swiftness, and encouragement. Greatest thanks to my family for their love and patience.

Contents

List of Figures

Chapter 1

Abstract

Concentrations of CO_2 in the mid-troposphere retrieved by NASA's Atmospheric Infrared Sounder (AIRS) were examined in relation to surface carbon dynamics, vegetation phenology, and precipitation (PPT) in the central US. Wavelet multi-resolution analysis was applied and the information theory metric of relative entropy computed for comparisons of eddy covariance tower CO_2 measurements at three sites in Northeastern Kansas with different land cover types. Sites experiencing woody encroachment agreed with AIRS mid-tropospheric CO_2 on a four-day time scale, while the tallgrass prairie site showed agreement at one month. Local, surface CO_2 measurements and regional PPT and normalized difference vegetation index (NDVI) values show greatest correlations with AIRS mid-tropospheric CO_2 at the 18-month scale. AIRS observations agree with regional PPT and NDVI at seasonal and interannual scales suggesting that AIRS CO_2 measurements can be used to assess regional source-sink dynamics related to climate forcings.

Chapter 2

Introduction

Terrestrial ecosystem dynamics influence the Earth's climate system (Pielke et al., 1998), which is affected by variations in the concentration of atmospheric carbon dioxide (CO_2). CO_2 is the primary greenhouse gas (GHG) associated with anthropogenic climate change due to the combustion of fossil fuels (Davis and Caldeira, 2010). Geographic distribution of anthropogenic sources from fossil fuel emissions and land use change are difficult to assess due to ecosystem heterogeneity and the complex, human and natural processes involved in carbon release and uptake (Gurney et al., 2009). A recent study by Xiao et al. (2011) estimates that up to 40% of US fossil fuel emissions may be absorbed by natural ecosystems across the US, where net ecosystem exchange (NEE) of carbon results in a carbon sink of approximately 0.63 Pg C yr^{-1}.

However, biogeophysical and biogeochemical processes related to climate change, extreme weather events, and natural and anthropogenic disturbances cause interannual variation in NEE of CO_2. Understanding how different processes influence these variations requires the identification of temporal and spatial scales of carbon dynamics within ecosystems.

Natural and anthropogenic sources of CO_2 around the globe contribute to mid-tropospheric concentrations, and so far only natural ecosystems can mitigate these emissions. This mitigation requires the assistance of synoptic systems that distribute CO_2 along atmospheric fronts and atmospheric boundary layer (ABL) mechanisms that make it available for photosynthesis. Assuming that information related to CO_2 concentrations can flow between synoptic, ABL, and turbulent subsystems on a daily to subdaily time scale (Li et al., 2010; Ruddell and Kumar, 2009a), changes in soil moisture, surface albedo, and temperature that drive biosphere-atmosphere interactions at short time scales will also influence mid-tropospheric CO_2. Casso-Torralba et al. (2008) quantify the importance of vertical and horizontal advective flux of daytime CO_2 concentration. Entrainment of the free troposphere can dilute or increase CO_2 concentration in the ABL. On a daily time scale, entrainment of air masses from the free troposphere and vertical transport caused by turbulent fluxes seem to have a greater influence on the early morning temporal evolution of CO_2 concentration in the ABL than plant uptake from photosynthesis (Casso-Torralba et al., 2008; Gibert et al., 2007).

Variations in photosynthesis and respiration that drive the larger amplitude of diurnal and seasonal carbon cycles associated with vegetation growth and senescence within the ABL have been captured by eddy covariance (EC) tower measurements and are well documented (Baldocchi, 2008). EC towers perform best on a flat topography with uniform vegetation and steady atmospheric conditions, and an increase in systematic bias errors can occur within heterogeneous landscapes. Advection of heat and moisture influence turbulent mixing and the vertical exchange of CO_2 between the ABL and the free troposphere, which can add to the difficulty of measuring carbon fluxes over complex terrain (Baldocchi, 2008). Still, errors associated with annual carbon-budget measurements by the eddy covariance method are considered

minimal and in the range of 30-100 gCm^{-2} $year^{-1}$, "less than a 1 m^2 paper weighing 76 g" according to Baldocchi (2008).

Although diurnal and seasonal variations in surface carbon cycling are well known, processes influencing patterns of CO_2 in the mid-troposphere have so far focused on synoptic weather and large scale atmospheric dynamics (Jiang et al., 2010; Li et al., 2010). The temporal and spatial dynamics of NEE as seen from CO_2 concentrations within the mid-troposphere have yet to be examined. It is important to keep in mind what greater CO_2 concentration at the surface means versus greater CO_2 concentration in the mid-troposphere. At the surface, it implies lower levels of photosynthesis, the process of carbon uptake by plants, or higher levels of respiration, CO_2 release by plant and microbial communities. Decreased photosynthesis and increased respiration corresponds with the end of the growing season and plant senescence or greater microbial activity associated with higher soil moisture and temperature as well as increased leaf litter (Scott et al., 2006). In the mid-troposphere, greater CO_2 concentration means that the rising global signal, coming from various local and regional sources, is being redistributed according to synoptic weather patterns and surface processes near, though maybe not at, the study location.

In an effort to advance studies of carbon dynamics, national and international observatory networks, such as AmeriFlux, the National Ecological Observatory Network, Inc. (NEON), and FLUXNET, have been established to combine local surface measurements from over 400 EC towers worldwide (Baldocchi, 2008). Although the average footprint of these towers are on the order of 1 km^2, these surface measurements have been used to up-scale CO_2 concentrations and fluxes to provide estimates of gross primary productivity (GPP) and NEE on regional to continental scales (Jung et al., 2009; Xiao et al., 2011).

In addition, reliable methods of monitoring CO_2 concentrations at a regional scale

(approximately 10^4 to 10^6 km^2) are needed for developing policies to regulate CO_2 emissions (Davis and Caldeira, 2010). Land use management practices, especially those related to agriculture and forestry, have the potential to mitigate or add to global emissions. Different biomes react uniquely across time and space to climate forcings of precipitation and higher levels of CO_2 (Stoy et al., 2009). Therefore, global and local policies may be inadequate, even detrimental, for ecosystem functioning at regional scales. For example, Koster et al. (2004) identified regional hotspots of soil-moisture and precipitation feedback around the globe. If carbon dynamics within these regions are shown to have a mitigating influence on the global carbon balance, national policymakers will want to focus their efforts on maintaining these ecosystems.

Satellite instruments are also being developed and launched, and some have already released global, daily data of CO_2 concentration in the mid-troposphere (Boesch et al., 2011; Jiang et al., 2010). In December of 2009, mid-troposphere retrievals of CO_2 concentrations from the Atmospheric Infrared Sounder (AIRS) instrument, onboard the NASA Earth Observing System Aqua satellite from 2002 on, were made available. Initial analyses of radiance measurements showed promising results, and comparisons of retrievals to transport models, aircraft flasks, and Fourier Transform Infrared Spectrometer measurements indicated an accuracy of 1-2 ppmv (Chahine et al., 2008; Maddy et al., 2008).

Comparisons of surface and atmospheric measurements are key to understanding CO_2 concentrations and flux dynamics within heterogeneous landscapes and complex, nonlinear processes related to carbon cycling and climate change. Analyses also must overcome challenges associated with differing spatial scales, such as different measurement resolutions (Brunsell and Gillies, 2003), and data availability due to different data processing methods, instrument limitations, and occasional malfunctions (Baldocchi et al., 2000). Additional difficulties in quantifying regional, net CO_2

concentrations and fluxes arise from the nonlinear influences of environmental variables, such as air temperature and soil moisture, at the microscale that can alter processes of photosynthesis and respiration (Monson et al., 2005). Long-term, combined observations of surface and atmospheric CO_2 offer the potential for a better understanding of the natural processes and anthropogenic activities related to CO_2 source-sink dynamics, seasonal and interannual variability, and climate forcings such as precipitation.

The detection and prediction of climate change in Kansas is complicated due to the natural interannual variability characteristic of this region (Brunsell et al., 2010). Averaged over the state, Brunsell et al. (2010) found that long-term observations from the 20th century indicate that climate in Kansas has been fairly stable. Seasonal trends in temperature for 1950-2000 are not found to exhibit clear spatial organization along latitude or longitude coordinates. However, irrigation in Western Kansas may result in increasing atmospheric moisture and cooling, which can affect both local evapotranspiration and regional precipitation patterns and mask predictions of increased temperatures and decreased precipitation across the Great Plains Brunsell et al. (2010).

This study seeks to comprehend how CO_2 concentrations in the mid-troposphere are related to local, surface CO_2 concentrations, and regional precipitation and vegetation phenology. Two questions related to the temporal dynamics surrounding local and regional scale CO_2 concentrations are examined: (1) How are temporal scales of CO_2 in the mid-troposphere related to surface CO_2 fluxes in a complex, regional landscape, such as grasslands with woody encroachment in northeastern Kansas? and (2) Do seasonal variations in mid-troposphere CO_2 correlate with seasonal variations in regional precipitation and remotely sensed measures of phenology in the Great Plains? It is hypothesized that (1) mid-troposphere CO_2, compared to surface CO_2, will ex-

hibit daily and seasonal temporal lags and decreased amplitude in flux dynamics, and that (2) seasonal variations of CO_2 in the mid-troposphere will correlate with temporal variations in precipitation and NDVI on a regional scale. The purposes of this comparative study are to better illustrate surface-atmosphere CO_2 fluxes at the local to regional scales, to contribute to the understanding of NEE of CO_2 over complex landscapes, to identify the dominant temporal scales at which processes may actively transport and distribute CO_2 at the surface and in mid-troposphere, and to assess the utility of mid-tropospheric CO_2 measurements for local to regional source/sink dynamics given climate forcings of precipitation and anthropogenic CO_2.

To examine whether AIRS CO_2 measurements in the mid-troposphere are representative of concentrations at the land surface below, three eddy covariance (EC) towers were selected at sites with different types of vegetation cover in Northeastern Kansas. Two of the towers are located at the Konza Prairie Biological Station and have been collecting data since 2006, while the third is located at the Kansas Field Station collecting data since 2007. All three towers are 3 m in height and are maintained by the Biometeorology Lab at the University of Kansas, where data is also processed. The towers on the Kansas Field Station and on watershed site 1D of the Konza Prairie Biological Station are part of the AmeriFlux network. Due to the availability of the EC data, this part of the analysis was limited to years 2007-2010.

In the second part of the analysis, concentrations of AIRS mid-tropospheric CO_2 were compared to NOAA Climate Prediction Center US Unified Precipitation (PPT) data and to the Moderate Resolution Imaging Spectroradiometer (MODIS) data of Normalized Difference Vegetation Index (NDVI) across the Great Plains for years 2002-2010. This broader spatial scale allowed for a more regional assessment of how differences in environmental variables like PPT and NDVI relate to mid-tropospheric CO_2.

Methods of lagged correlation, wavelet multi-resolution analysis, and the information theory metric of relative entropy were applied to ascertain relationships between mid-troposphere CO_2 concentrations and surface CO_2 concentrations, PPT, and NDVI. While lagged correlations identify time scales where one variable lags or leads another, wavelet multi-resolution analysis can reveal the time scale at which a decomposed version of a field is contributing the most to the original, observed time series of another field. The relative entropy metric provides a means of evaluating the agreement between two variables to determine how representative one can be of the other. Taken together these methods help elucidate temporal scales and spatial patterns to further the understanding of processes involved in climate change at a regional scale, especially relationships between global, atmospheric CO_2 concentrations and local or regional ecosystems.

2.1 Background

Scientific interest in atmospheric CO_2 concentration, its variation in the carbon cycle and as a climate forcing, are found in the literature starting in the nineteenth century when the accuracy of recorded measurements from sampling stations was already debated (Arrhenius, 1896; Billings, 1893; Callendar, 1940; Keeling, 1960; Willis, 1901). Quantifying local to regional sources and sinks of atmospheric CO_2 around the globe continues to be one of the greatest challenges facing climate science today. The first direct observation from space of the interannual increase in CO_2 from 2003 to 2005 was made fairly recently (Buchwitz et al., 2007) and has opened up new possibilities for monitoring CO_2 within our Earth's systems.

Observations of atmospheric CO_2 concentrations from satellite instruments hold great potential for filling global data gaps, especially in regions lacking surface-based

observations. The eddy covariance method allows seasonal CO_2 fluxes to be quantified at a local scale, on the order of 100 m^2, but this method cannot account for lateral transport of carbon, carbon losses to groundwater, or export of carbon through harvest and fire (Baldocchi, 2008; Schulze, 2006). While satellite data may capture advection of CO_2 at the global scale, it is important to know whether such data can also be used to identify sinks and sources within geopolitical boundaries.

Estimations of terrestrial carbon exchange have been obtained through various methods including top-down approaches that use global- to regional-scale, atmospheric concentration measurements to model or estimate sink and source activity, and bottom-up approaches that scale up from local, surface flux measurements and model related processes. Top-down observations that start at a continental scale and attempt to scale down are limited by the complexity of heterogeneous landscapes, for example. Bottom-up studies that start at the micro scale encounter difficulties when scaling up to represent complex regions of study. Both top-down and bottom-up approaches are further restricted by the lack of theoretical knowledge in scaling nonlinear processes related to ecosystem fluxes (Lai et al., 2006; Peters et al., 2005). Riley et al. (2009) predict that a combination of top-down and bottom-up approaches and boundary layer budgeting are necessary to evaluate NEE estimates, especially over complex landscapes.

Numerous studies call for the continued development of process-based carbon-climate models that incorporate the latest parameters of hydrologic and carbon cycling at regional scales (Desai, 2010). Tiwari et al. (2006) indicate that AIRS CO_2 data can be used to improve representation of CO_2 transport from the lower to upper troposphere in current models used for carbon accounting. In contrast to previous assumptions, AIRS observations analyzed by Chahine et al. (2008) have shown that CO_2 is not well mixed in the mid-troposphere (between 8 and 13 km). At this level,

tropospheric weather and large-scale circulation patterns affect CO_2 distribution. For example, strong gradients are seen at 45°N in correlation with the mid-latitude jet stream in the Northern Hemisphere. AIRS observations south of the mid-latitude jet stream between 30°N and 40°N are high in comparison with measurements north of the jet stream, and spatial gradients of 2-3 parts per million by volume (ppmv) are seen across the United States. In addition, Jiang et al. (2010) have demonstrated that interannual variability of mid-tropospheric CO_2 is related to the El Niño Southern Oscillation (ENSO) and the polar vortex. Li et al. (2010) provide further insight to the vertical transport of CO_2 related to the Madden-Julian oscillation. They suggest that areas with enhanced upward or downward motions associated with large-scale circulations can transport CO_2 from the atmospheric boundary layer (ABL) to the troposphere or vice versa on the time scale of a day.

The temporal and spatial scales of CO_2 transport between the land surface, the ABL, and the free troposphere vary widely, and there is limited understanding of the processes involved. So far, it is understood that daily evolution and atmospheric distribution of CO_2 are driven by biosphere-atmosphere interactions (Casso-Torralba et al., 2008; Li et al., 2010). This means that the CO_2 mixing ratio in the ABL is influenced by surface fluxes and meteorological processes that mix free-tropospheric air into the ABL. Parazoo et al. (2008) demonstrate that in mid-latitudes 60-70% of CO_2 variation in the ABL throughout the year can be attributed to advection, less than 5% is caused by moist convection, and the remainder is related to surface fluxes. Soil and vegetation processes, such as evapotranspiration, photosynthesis, respiration, and the entrainment of tropospheric air during ABL growth affect the concentration of CO_2 in the ABL on a local scale. In turn, dynamics involved in cloud formation and mesoscale circulations influence the distribution of atmospheric CO_2 on a regional scale (Casso-Torralba et al., 2008; Helliker et al., 2004).

The amount of CO_2 at any point within the ABL is a function of the composition of the original air masses during ABL formation, exchanges with the land surface, and exchanges with the troposphere, all driven by variables like land cover type and soil moisture. Given the role of the ABL as a filter of information between surface and mid-tropospheric measurements of interest, it is important to mention other physical processes that affect transport of CO_2 within the ABL. For example, horizontal transport within the ABL is estimated to move over the land surface at 500 km day^{-1} and the surface area influencing the concentration of a trace gas in the ABL, such as CO_2, ranges from 10^3 to 10^5 km^2 (Styles et al., 2002). In addition, Cotton et al. (1995) estimate that vertical transport from convective storm processes around the globe completely replaces the air masses in the ABL approximately 90 times per year, or every four days.

Mesoscale convective systems, deep convective systems that have a horizontal dimension of about 200 km up to 1000 km and a typical lifetime of 6 to 12 hours, can transport CO_2 between the ABL and the mid-troposphere. They possess complex, slantwise ascending and descending flow branches that along with cumuli can vent a substantial amount of ABL air up to the free troposphere. Vented air can then be replaced by mid-tropospheric air carried down by convective downdrafts or mesoscale air streams that slowly descend. A large percentage of the rain that falls back to the surface during a mature, mid-latitude mesoscale convective system is water injected into the middle and upper troposphere (Cotton et al., 1995).

Vertical transport of atmospheric compounds, such as CO_2, from the ABL to the free troposphere is further influenced by cloud formation. Shallow cumuli and fair weather clouds change the structure and growth of the ABL which can enhance the development of thermal chimneys responsible for the vertical transport of CO_2 emitted at the surface. Cloud venting is the process by which gaseous matter and aerosols

are transported from the lower troposphere to the middle and upper troposphere. The fate of the CO_2 particle that is vented from the ABL to the middle troposphere is therefore dependent on air movement associated with cloud formation and the precipitation processes of that cloud or cloud system (Cotton et al., 1995). A need to study the dynamics and coupling of the cloud and subcloud layer that are involved in this venting remains (Chaumerliac and Leriche, 2000).

Consideration of surface heterogeneity or land cover type is crucial to evaluating measurements of CO_2 concentrations at the surface, and it may also play a significant role in mid-tropospheric measurements. In areas experiencing woody encroachment or reforestation, increased leaf litter may cause greater microbial respiration rates, especially after precipitation events (Scott et al., 2006). At nighttime the flow of CO_2 around the soil and vegetation often becomes decoupled from the atmosphere above. So, when turbulent mixing reinitiates at sunrise, respired CO_2 that has been stored in the vegetation and surface layer can be vented to the free troposphere meaning that large amounts of CO_2 can be vented on very short time scales (Baldocchi, 2008).

Regional NEE of carbon can also be strongly coupled with hydrological processes (Brunsell, 2006; Desai, 2010; Ruddell and Kumar, 2009a,b). With adequate soil moisture, ecosystem respiration increases with temperature (Reichstein et al., 2003, 2005). Surface heterogeneity in soil moisture also affects the growth of the ABL, cloud formation, and moist thermodynamic conditions that alter the surface fluxes (Entekhabi et al., 1996; Findell and Eltahir, 2003). Jones and Brunsell (2009) found that in the US Central Plains a positive feedback between soil moisture and precipitation occurs based on energy balance partitioning of sensible and latent heat. This confirms the identification by Koster et al. (2004) of this region as a global hotspot for feedbacks between soil moisture and precipitation.

Anthropogenic disturbances of Great Plains ecosystems alter CO_2 source-sink dy-

namics. Land management practices related primarily to ranching and agriculture have the potential to mitigate or add to emissions around the globe. Human and natural system couplings add to the complexity of evaluating influences of land cover on CO_2 concentrations, as land use practices and decisions are nonlinear and vary across time, space, and structural domains (Lambin and Meyfroidt, 2010; Liu et al., 2007). Complex patterns and processes arise from the influence of humans on landscape heterogeneity and on various feedback loops, time lags, and thresholds in human and natural systems. For example, agricultural land-use transitions across the Great Plains are influenced by both endogenous socio-ecological feedbacks, due to disturbances, degradation, and resource depletion observed on local scales, as well as exogenous socio-economic changes and innovations driven by international markets independent of the local ecological systems (Lambin and Meyfroidt, 2010). Assessment of local to regional scale carbon budgets ultimately requires an understanding of human-nature system complexities. Though this study does not directly address such complexities, land management practices undoubtedly play a role in carbon dynamics in northeastern Kansas and the Great Plains region.

Annual burning became a land management practice in the grasslands of the Great Plains in part to control the expansion of invasive species, such as *Cornus drummondii* (roughleaf dogwood) and *Juniperus virginiana* L. (eastern redcedar). Shrub and tree encroachment leads to increased short-term carbon storage above ground, but these pools are vulnerable to fires and changes in land use. Water availability, vegetation distribution, and rooting depth are important factors in ecosystem carbon dynamics related to woody encroachment (Potts et al., 2006; Scott et al., 2006).

Bremer and Ham (2010) found that controlled annual burning of grasslands increases carbon loss compared to biennial burning, especially at times of above average

precipitation. This occurs because of greater respiration rates at the end of the growing season from increased biomass resulting from the burn and greater precipitation earlier in the year. Less frequent burning (up to approximately every four years) is suggested as a land management strategy for mitigating climate change, and is not predicted to support woody encroachment if trees and shrubs are "burned before becoming too large" (Bremer and Ham, 2010).

Free-range grazing by ungulates is not only an alternative to burning regimes, but may also be a way that ranchers in the Great Plains can participate in CO_2 mitigation in this region (Owensby et al., 2006). Characterized by increased photosynthesis in younger leaves and an open canopy accompanied by significantly lower soil respiration rates, grazed plots in a study by Owensby et al. (2006) were found to be carbon neutral. Unfortunately, cattle raised in feedlots may contribute substantially to increased CO_2 concentration and flux measurements in the region (Baum et al., 2008). In a footprint of approximately 1 km^2, 61% of CO_2 fluxes where attributed to a nearby feedlot.

Finally, agriculture has continued to succeed in semi-arid regions of the Great Plains even after the Dust Bowl due in part to the advancement of technology for groundwater irrigation from the High Plains Aquifer. Speculation that irrigation in areas like Western Kansas has been changing precipitation patterns in the Great Plains has existed for over 30 years (Brunsell et al., 2010; Schickedanz, 1976). During the last decade, a wet trend throughout the growing season, warming temperatures, nitrogen deposition, and fertilizer have resulted in greater NPP in northern mid-latitudes (Zhao and Running, 2010). Ruddell and Kumar (2009a) have shown that as long as agricultural systems are in a healthy, non-drought state, energy in the form of sensible and latent heat as well as water vapor are exchanged via turbulent and ABL subsystem feedback loops and influence regional-scale weather and carbon dynamics

on a local to regional scale (Ruddell and Kumar, 2009a).

2.2 Region of Study

The study area spans the US Great Plains, lying east of the Rocky Mountains and west of the Mississippi River. It extends from 88.75°W to 103.75°W and 31°N to 45°N as shown in Figure 2.1. The Great Plains are characterized by temperate grasslands, savannas, and shrublands starting in the west and covering much of the region and transitioning to temperate broadleaf and mixed forests in the eastern states. Most of the regions native prairies, from short grasses in the west, mixed grasses in the central plains, and tall grasses in the east, have been converted for agriculture. A cold, semi-arid climate in the northwest turns to a warm, semi-arid climate in the southwest, while north central and northeastern states have a humid continental climate and south central and southeastern states exhibit a humid subtropical climate. A precipitation gradient exists across the region increasing from west to east often delineated by the 100th meridian that separates the humid and semi-arid climatic regions.

2.2.1 Grassland Sites

The Nelson Environmental Study Area (39°N, 94°W) is comprised of 560 acres within the Kansas Field Station (KFS) owned by the University of Kansas. KFS is located north of Lawrence, Kansas, in a tallgrass prairie and deciduous forest ecotone. The eddy covariance (EC) tower at this site started collecting data on July 15, 2007, and is within an abandoned grassland currently dominated by C_3 grasses, such as smooth brome (*Bromus inermis* Leyss), tall fescue (*Festuca arundinacea* Schreb.), and Kentucky bluegrass (*Poa pratensis* L.). Native grasses, forbs, and woody species

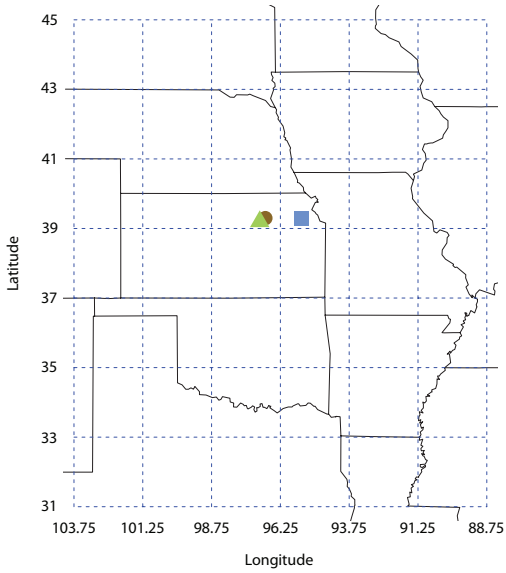

Figure 2.1 Region of study with AIRS pixel grid and KFS (blue square), KZU (brown circle), and K4B (green triangle) tower locations.

are also present, and the soils are fine, montmorillonitic, mesic Aquic Argiudolls. From 1987 to 2007 this area was burned approximately every five years and has been experiencing woody encroachment (Brunsell et al., 2011). Mean annual temperature in this temperate, mid-continental climate is 13°C, and mean annual precipitation is 937 mm.

The Konza Prairie Biological Station (39°N, 96°W) is a field research station on 8,600 acres south of Manhattan, Kansas, jointly owned by The Nature Conservancy and Kansas State University. Konza is located within the Flint Hills region known for flint-bearing limestone layers, and soils are fine, mixed, mesic Udic Argiustolls. This area is composed of native tallgrass prairie with primarily perennial C_4 grasses, such as big bluestem (*Andropogon gerardii* Vitman), little bluestem (*A. scoparius* Michx.), and indiangrass (*Sorghastrum nutans* [L.] Nash), and other sub-dominant grasses, forbs, and woody species. The AmeriFlux eddy covariance tower, designated as tower KZU, is located on watershed site 1D that has been burned annually for

several decades and has not been grazed for more than 30 years (Bremer and Ham, 2010). Data from another EC tower located on watershed site 4B, a mix of C_3 forbs and C_4 grasses burned every four years, are also used in the analysis. Referred to as K4B, the different vegetation and burning regime at this site broaden the scope of the study by adding a third land cover type to the comparison between surface and mid tropospheric CO_2. Mean annual temperature for this area, like the KFS site, is 13°C. The mean annual precipitation is 835 mm, slightly less than the more eastern KFS site and characteristic of the Kansas precipitation gradient decreasing from east to west.

Chapter 3

Data

3.1 Eddy Covariance Towers

The eddy covariance technique is used to measure the net ecosystem exchange of CO_2 between the biosphere and the atmosphere (Baldocchi et al., 2001). Micrometeorological EC towers measure fluxes of energy, water vapor, and carbon dioxide covering a longitudinal length of 100-2000 m depending on sampling height and atmospheric conditions (Baldocchi et al., 2001). FLUXNET was established in 1998 as a global network of long-term measurement sites, in part to validate NASA Earth Observing System (EOS) products. In this study, surface EC measurements can help identify the time scales at which surface CO_2 agree with mid-tropospheric measurements from NASA's Atmospheric Infrared Sounder. CO_2 and water vapor concentrations are measured with an open path infrared gas analyzer with wind speeds from a sonic anemometer at 20 hz. Data are collected by a Campbell Scientific CR 3000 Datalogger. The data are processed in a standard way (see Baum et al. (2008) for details on the post-processing algorithm), including a coordinate rotation using the planer fit method (Wilczak et al., 2001) as well as the standard corrections for density (Webb

et al., 1980) and sonic-anemometer derived estimates of temperature (Schotanus et al., 1983). In addition, corrections are made for despiking and lag removal, as well as correcting for sonic temperature heat flux for humidity, sensor separation, and spectral attenuation. Daily averages of CO_2 concentration for 2007-2010 are calculated from 48 half-hour measurements in a 24-hour period for comparison with AIRS daily observations. Missing daily values for all three EC towers (18.57% at KFS; 6.43% at KZU; 5.16% at K4B) are replaced with weekly means, and monthly means when weekly data are not available.

3.2 Atmospheric Infrared Sounder

The Atmospheric Infrared Sounder (AIRS) was launched on NASA's EOS Aqua satellite on May 4, 2002. At an altitude of 705 km, this polar orbiting instrument had an expected on-orbit lifetime of seven years and continues to provide global coverage twice daily at equatorial cross times of approximately 1:30 am and 1:30 pm. These daily observations have a nadir resolution of 90 km x 90 km and are regridded to a spatial resolution of 2.5° longitude by 2° latitude for the AIRS Level 3 product. CO_2 retrievals are from the 15-μm, thermal infrared band, and selected cloud-cleared channels are used. The peaks of the weighting functions for the CO_2 channels occur between 500 hPa and 300 hPa (Jiang et al., 2010). Comparisons of retrievals to transport models, aircraft flasks, and Fourier Transform Infrared Spectrometer measurements indicate an accuracy of 1-2 ppmv (Chahine et al., 2008; Maddy et al., 2008). Engelen and McNally (2004) applied information theory to examine the accuracy of AIRS retrievals and found a column-averaged mixing ratio error of 1.2 ppmv. In addition, a 10% error caused by water vapor in AIRS retrievals can also cause a 1-ppmv bias in CO_2 (Chahine et al., 2005).

As a first step in the study, AIRS mid-troposphere CO_2 concentrations were compared with observed CO_2 via eddy covariance at the surface. A time series of AIRS Level 3 daily observed CO_2 was obtained for 2007-2010 to correspond with EC tower data, 1260 days in total. The AIRS pixels that most closely cover the KFS and Konza towers were selected: 95°W, 40°N and 97.5°W, 40°N, respectively. Due to a high percentage of missing daily values (50.48% for the AIRS pixel over KFS and 47.94% for the AIRS pixel over Konza), the mean of the entire series for each pixel is used to fill in missing daily concentrations.

The next step was to assess ecosystem dynamics across the Great Plains region. AIRS Level 3 CO_2 data from 2002 to 2010 were compared with Normalized Difference Vegetation Index (NDVI) and precipitation data across the area of study. Daily AIRS values were averaged over a 16-day period to correspond with the temporal scale of MODIS NDVI data starting on day of year (DOY) 249 in 2002 and ending on DOY 361 in 2010. AIRS' spatial scale of 2.5° longitude by 2° latitude is the coarser resolution of the data sets, requiring both NDVI and precipitation data to be aggregated. Given the extent of the area of study, from 88.75°W to 103.75°W and 31°N to 45°N, a total of 42 pixels were evaluated (Figure 2.1).

3.3 MODIS Normalized Difference Vegetation Index

The Normalized Difference Vegetation Index (NDVI) is calculated from surface reflectance from the red (R_{RED}) and near-infrared (R_{NIR}) parts of the spectrum given by

$$NDVI = \frac{R_{NIR} - R_{RED}}{R_{NIR} + R_{RED}}. \tag{3.1}$$

The index is a direct indication of vegetation and cover density, where larger values

of NDVI usually correspond to higher vegetation productivity.

Data for NDVI were acquired from the Moderate Resolution Imaging Spectroradiometer (MODIS) instrument, also aboard the NASA EOS Aqua satellite. Data is provided as a level 3 product by the US Geological Survey (USGS) and projected on a geographic Climate Modeling Grid (CMG) with a spatial resolution of 0.05° longitude by 0.05° latitude. Starting on DOY 9, values of NDVI corresponding to 16-day intervals are given. Spatial composites are selected by an algorithm for the most cloud-free and closest to nadir pixel within a 16-day collecting period. The last 16-day value on DOY 361 is computed from the last five to six days of the year and the first eleven to ten days of the following year, though the first annual value always starts on DOY 9. For this study, data were examined from DOY 249 in 2002 to DOY 361 in 2010. The global data set was aggregated to match the AIRS pixels.

3.4 NOAA Climate Prediction Center Unified Precipitation

NOAA Climate Prediction Center US Unified Precipitation data were obtained for years 2002 to 2010 from NOAA/OAR/ESRL PSD, Boulder, Colorado, USA (http://www.esrl.noaa.gov/psd/). Daily values are available at a resolution of 0.25° longitude by 0.25° latitude. To match the temporal scale of the 16-day NDVI composites, precipitation (PPT) was summed over 16 days from DOY 249 in 2002 to DOY 361 in 2010 over the subset of the region of study. Data were then aggregated to match the spatial scale of AIRS, and the mean of all original pixel values was used.

Chapter 4

Methods

In both parts of the analysis, the comparison of local EC tower measurements to AIRS observations and the broader examination of mid-troposphere CO_2, NDVI, and PPT in the Great Plains region, the traditional technique of lagged correlation was initially applied to explore temporal lags. Lags of 180 days were examined in the EC-AIRS comparison, and lags of 50 16-day periods or a total of 800 days were used to evaluate temporal relationships between mid-troposphere CO_2, NDVI, and PPT. The interannual linear trend for AIRS CO_2 and seasonality for AIRS CO_2, NDVI, and PPT were removed for this part of the analysis.

A wavelet multi-resolution analysis combined with the information theory metric of relative entropy following Brunsell (2010) was then used to examine EC and AIRS time series to ascertain the relationship between surface and atmospheric measurements and between AIRS, NDVI, and PPT to better understand how mid-tropospheric observations relate to changes in vegetation phenology and precipitation at the surface. Wavelet analysis is a powerful tool that can be used to study nonstationary, geophysical processes with multi-scale features to extract information about or represent processes with simultaneous consideration of local and global cli-

mate signals (Baldocchi et al., 2000; Kumar and Foufoula-Georgiou, 1997; Lau and Weng, 1995; Torrence and Compo, 1998). In this study, the variability of precipitation, changes in vegetation phenology, and CO_2 concentration at the surface and in the mid-troposphere were quantified as a function of temporal scale. Precipitation, NDVI, and surface and mid-troposphere signals of CO_2 were compared at each level of decomposition.

Wavelet analysis works through dilation (m) and translation (n) of a mother wavelet (ψ), in this case a Daubechies least-assymetric eight wavelet, to achieve a high level of localization in both the time and frequency domains. The wavelet transform is found by

$$W(m,n) = \lambda_0^{-m/2} \int_{-\infty}^{\infty} f(t)\psi(\lambda_0^{-m}t - nt_0)dt \tag{4.1}$$

where λ_0 is the initial scale of decomposition, and the wavelet is defined by

$$\psi_{m,n}(t) = \frac{1}{\lambda_0^m}\psi(\frac{t - nt_0\lambda_0^m}{\lambda_0^m}) \tag{4.2}$$

Windows of high localization are wide when looking at low-frequency signals and narrow when examining high-frequency signals. This zoom-in capability allows one to see brief, high-frequency events and resolve low-frequency variability in a time series (Lau and Weng, 1995).

Following Brunsell (2010), the relative contributions from each level of decomposition can be obtained by reconstructing the original signal

$$f(t) = \sum_n \sum_m D_{m,n}\psi_{m,n}(t) \tag{4.3}$$

where $D_{m,n}$ represents the wavelet coefficients. In addition, the original time series

(X) can be reconstructed based on

$$X(t) \approx \overline{X_m(t)} + \sum_{m \geq m_0} X'_m(t) \tag{4.4}$$

using residual fluctuations (X') at each point t. The multi-resolution decomposition results in wavelet subsignals or band-pass filtered renderings of EC tower, AIRS, NDVI and PPT time series at each scale of interest to be examined for spatiotemporal variations.

For the first part of the analysis, wavelet versions were decomposed to nine temporal scales corresponding to 2, 4, 8, 16, 32, 64, 128, 256, and 512 days. Correlation coefficients between original, undecomposed daily time series and wavelet decomposed versions of all three EC tower and corresponding AIRS time series were calculated for each temporal scale. In addition, correlations between wavelet decomposed versions of EC time series and wavelet decomposed versions of AIRS time series were examined at all temporal scales.

Across the Great Plains, correlation coefficients between original, undecomposed 16-day time series and wavelet decomposed versions of AIRS CO_2, NDVI, and PPT time series at each temporal scale were calculated. Time series were made up of 192 16-day periods, and wavelet versions were decomposed to seven temporal scales at 32, 64, 128, 256, 512, 1024, and 2048 days.

The information theory metric of relative entropy was also used to examine information gain and transfer, or the "temporal evolution of information flow" between land-atmosphere interactions (Brunsell, 2010; Brunsell and Young, 2008). The relative entropy $(R(x, y))$ represents the distance between the probability density func-

tions of variables x and y defined as:

$$R(x,y) = \sum_i p_i log(\frac{p_i}{q_i}) \tag{4.5}$$

where R is the additional amount of information needed to represent the probability density function (pdf) p associated with x given the probability of y in bin i determined from the pdf of q. In the first part of this study, the relative entropy between the EC tower and the AIRS observations was obtained, and the variability of CO_2 concentration at the surface versus the mid-troposphere was quantified as a function of temporal scale. Small values of relative entropy at a particular time scale signify that the pdf of the full signal is more closely approximated by the pdf of the decomposed version of the time series of the other field. The relative entropy metric can improve our understanding of surface-atmosphere interactions by identifying temporal scales where there is greatest agreement between original time series and wavelet decomposed versions of EC and AIRS CO_2, NDVI, and PPT.

Chapter 5

Results

5.1 AIRS and EC Tower Measurements of CO_2 in Northeastern Kansas

Original, daily time series of surface EC tower measurements and mid-troposphere AIRS observations of CO_2 concentration from 2007 to 2010 over KFS, KZU, and K4B sites are shown in Figure 5.1. AIRS time series exhibit less amplitude and seasonal variation in CO_2 concentrations than EC tower time series. Despite high missing daily values, a linear regression of weekly averages of the AIRS time series (orange lines) follows the increasing global trend in atmospheric CO_2 concentrations from approximately 384 ppmv in 2007 to approximately 394 ppmv in 2010. Small slope values indicate that mid-tropospheric CO_2 is rising in AIRS pixel 95W, 40N (slope=+0.00737 ppmv) and in AIRS pixel 97.5W, 40N (slope= +0.00673 ppmv). Linear regressions of weekly averages for the original EC time series were also computed (red lines). Slope values for original EC time series are also small, with KFS (slope=+0.0121 ppmv) and KZU (slope=+0.0137 ppmv) exhibiting small positive slopes and K4B (slope=-0.000523 ppmv) resulting in a small negative slope from

2007 to 2010. However, Buck and Brunsell (in preparation) have shown that, neglecting CO_2 released during burning regimes when towers are turned off, all three sites are net carbon sinks.

Root mean square error (RMSE) values between the original time series show a difference of 12.94 ppmv at KFS, 18.95 ppmv at KZU, and 13.96 ppmv at K4B. Once time series have been gap filled, RMSE values increase to 13.96 ppmv at KFS, decrease to 18.87 ppmv at KZU, and increase to 14.22 ppmv at K4B. Percent bias calculations show that AIRS mid-tropospheric observations exhibit a difference from surface concentrations of 1.3% at KFS, 1.6% at KZU, and 1.7% at K4B before gap filling. After gap filling these biases increase to 1.7% at KFS, 2.2% at KZU, and 2.2% at K4B.

Lagged correlations in Figure 5.2 give an initial assessment of the temporal relationships between surface and mid-tropospheric CO_2 concentrations. At the KFS site, the greatest negative correlation (-0.176) at which mid-troposphere CO_2 lag surface concentrations occurs at a seasonal scale (-118 days). On the other hand, the greatest positive correlation (0.191) where mid-tropospheric CO_2 leads surface concentrations occurs at a two-month scale (64 days). The relationship between mid-tropospheric and surface CO_2 at the KZU site shows mid-tropospheric CO_2 leading surface concentrations at both the two-month scale (48 days), with a positive correlation of 0.186, and at the six-month scale (170 days), with a negative correlation of -0.116. At site K4B, mid-tropospheric CO_2 both lags and leads surface concentrations at the seasonal scale where there is the greatest negative correlation (-0.273) at -132 days and the greatest positive correlation (0.237) at 118 days.

Correlations of the original time series and wavelet decompositions of the fields at each temporal scale (Figure 5.3) indicate that the greatest positive correlations between surface CO_2 and mid-tropospheric measurements occurs at the 18-month time

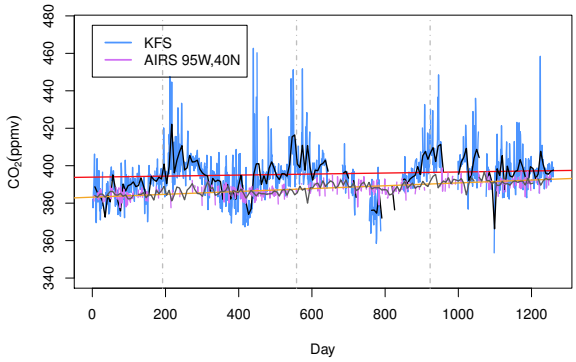

(a)

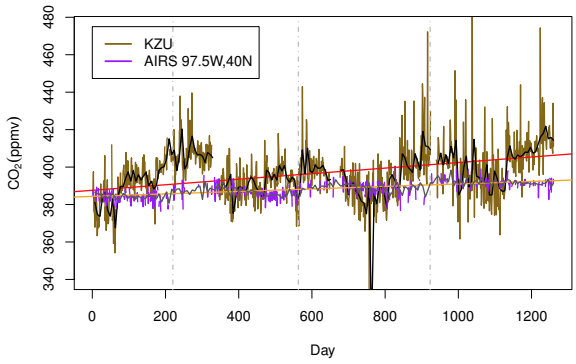

(b)

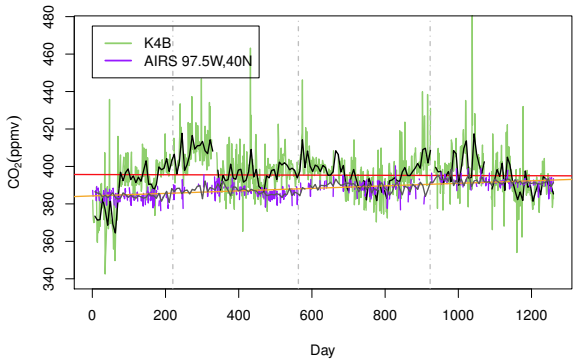

(c)

Figure 5.1 Time series of surface EC tower and mid-troposphere AIRS observations of CO_2 concentration from 2007 to 2010 over (a) KFS, (b) KZU, and (c) K4B.

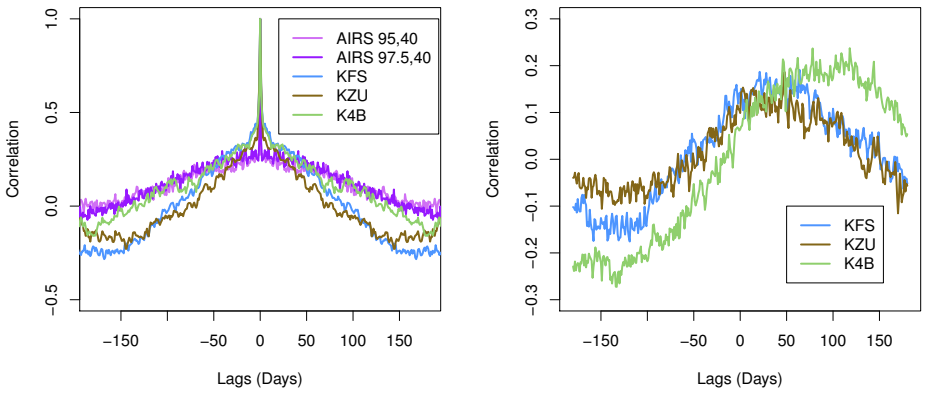

(a) **(b)**

Figure 5.2 (a) Lagged autocorrelation of the EC and AIRS time series and (b) lagged correlation between the EC and AIRS data.

scale (512 days). At correlation coefficients of 0.2 and above, wavelet decomposed versions of EC time series compared with the original AIRS time series of the corresponding pixels (Figure 5.3a) show that the KZU site best reflects the availability in mid-tropospheric CO_2 concentrations retrieved by AIRS on an 18-month scale compared to sites KFS and K4B. The reverse relationship, where wavelet decomposed versions of AIRS are compared to the original EC time series, also highlights the 18-month scale at which mid-tropospheric CO_2 may be exchanged with the land surface at the KZU site (Figure 5.3b). Comparing wavelet decomposed versions of both EC and AIRS time series (Figure 5.3c) reveals scales of greater contribution between surface and mid-troposphere CO_2 exchanges. Stronger positive correlations exist at the seasonal (0.555), annual (0.425), and 18-month (0.485) scales for site KFS and at the 16-day (0.245), two-month/64-day (0.234), and seasonal (0.265) scales for site KZU. Site K4B exhibits stronger negative correlations at the two-month (-0.356) and annual (-0.224) scales. The strong positive correlation (0.999) seen at the 18-month scale for site KZU and the maximum negative correlation of -1 at the three-year (1024

days) scale at all three sites are indicative of the lower reliability of longer time scales in wavelet multi-resolution analysis (Percival, 1995; Torrence and Compo, 1998).

Relative entropy (RE) of wavelet decomposed versions of the EC time series compared to the original AIRS time series, and wavelet decomposed versions of the AIRS time series compared to the original EC time series are shown in Figure 5.4. Lower relative entropy values correspond to greater agreement between time series, i.e. less additional information is needed to capture the observed pdf. The time scale for which surface CO_2 concentrations are best represented by the corresponding mid-troposphere AIRS pixel varies between sites (Figure 5.4a). Site KFS shows the best agreement at the four-day scale (RE=0.882), while site KZU shows the best agreement at time scales of one month/32 days (RE=0.810) and two months/64 days (RE=0.845). Site K4B shows good agreement with mid-tropospheric concentrations from the four-day to the seasonal scale, with lowest RE values occurring at the four-day (RE=0.665), 8-day (RE=0.839), and seasonal (RE=0.827) scales.

When assessing how well mid-tropospheric concentrations are represented by surface EC measurements (Figure 5.4b), the KFS site stands out as being representative of mid-tropospheric CO_2 at all but the four-day time scale. The best agreements between mid-troposphere CO_2 and KFS is seen at the 2-day (RE=0.138) and 8-day (0.440) scales, while the best agreements for the K4B site occur at the seasonal (RE=0.523) and annual (RE=0.678) scales. The lowest relative entropy values at the KZU site are seen at times scales of 16-days (RE=1.483) and two-months/64-days (RE=1.222).

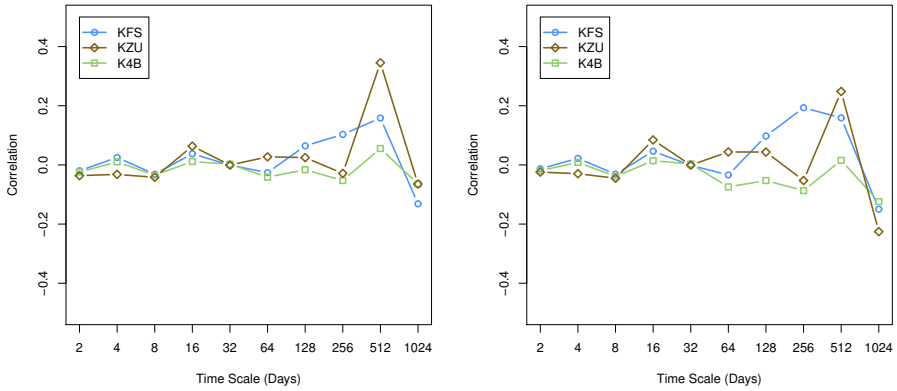

(a)

(b)

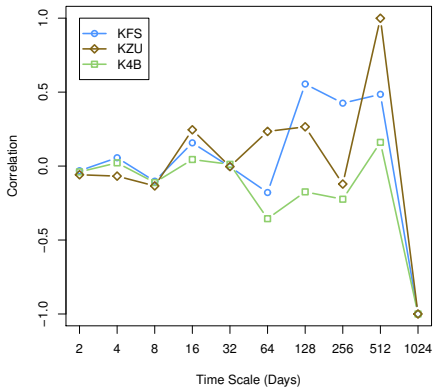

(c)

Figure 5.3 Correlations of (a) AIRS time series with wavelet decomposed versions of EC time series, (b) EC time series with wavelet decomposed versions of AIRS time series, and (c) wavelet decomposed versions of EC with wavelet decomposed versions of AIRS. Wavelets are decomposed to ten temporal scales corresponding to 2, 4, 8, 16, 32, 64, 128, 256, 512, and 1024 days.

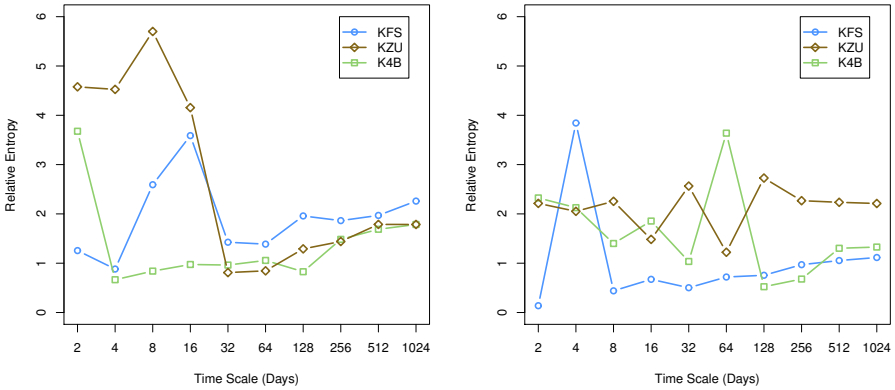

(a) **(b)**

Figure 5.4 Relative entropy of (a) AIRS time series with wavelet decomposed versions of EC time series and (b) EC time series with wavelet decomposed versions of AIRS time series. Lower relative entropy corresponds to greater agreement between time series.

5.2 AIRS CO_2, MODIS NDVI, and PPT in the Great Plains

Across the Great Plains region, time series of AIRS mid-tropospheric CO_2 exhibit a rising temporal trend from approximately 370 ppmv in late 2002 to over 390 ppmv by the end of 2010. AIRS, NDVI, and PPT time series also exhibit seasonality, with lower values of AIRS, and higher values of PPT and NDVI seen in the growing season. The CO_2 linear trend and the seasonality, determined by the mean for each 16-day value in all years, of all time series were removed for the lagged correlation part of the analysis, while original time series were used for the wavelet multi-resolution analysis and calculation of the relative entropy metric. Comparisons of mean annual AIRS CO_2 with mean annual PPT and mean annual max NDVI (Figure 5.5) show that greater annual PPT tends to correspond with lower annual CO_2 in the mid-troposphere. Greater annual maximum NDVI occurs parallel with lower values of

CO_2 in the southeast and slightly higher values of CO_2 in the mid to north latitudes in the eastern part of the region. Of most importance is the strong positive relationship between mean annual PPT and mean annual maximum NDVI, where greater PPT relates to higher levels of NDVI. Spatial variation is seen in these relationships and less PPT is associated with higher NDVI in the mid longitudes and northern latitudes, for example (Figure 5.5c).

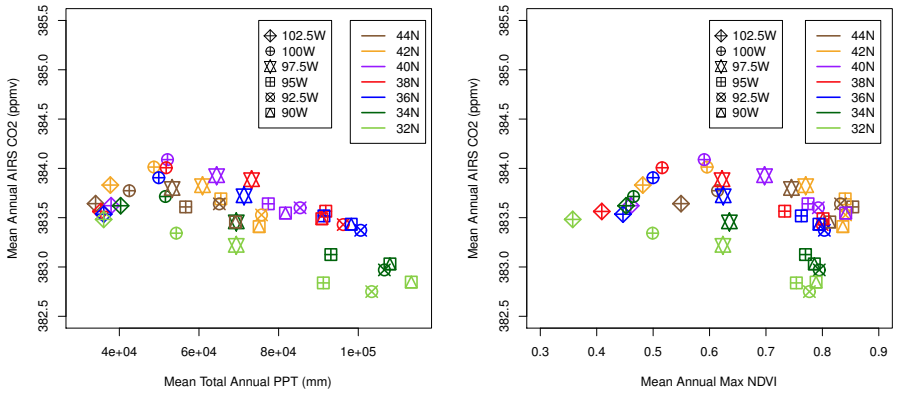

Figure 5.5 (a) Mean of AIRS CO_2 with mean annual PPT. (b) Mean of AIRS CO_2 with mean of maximum annual NDVI. (c) Mean annual PPT with mean of maximum annual NDVI.

Original NDVI time series show a general spatial trend of increasing values and seasonal variance from southwest to northeast, while original PPT time series display a known gradient increasing from west to east with greatest values in the southeast. To better illustrate spatial relationships among time series, temporal scales of greatest positive or negative correlations, or distribution between the two, and lowest relative entropy were selected and mapped. For example, the relative entropy metric calculated between wavelet decomposed versions and original time series indicates that there is greatest agreement between AIRS CO_2, NDVI, and PPT at longer time scales, particularly seasonal (128 days) and annual (256 days) scales. With a couple exceptions, results at these scales do not show an obvious geographic pattern across the region of study and, therefore, are not mapped.

Lagged correlations between AIRS and PPT and AIRS and NDVI are shown in Figure 5.6. While relationships between AIRS and PPT vary monotonically across the region, lagged correlations between AIRS and NDVI show a general trend of decreasing periodicity from west to east. The greatest positive correlation (0.300) between AIRS and PPT across the region occurs at 92.5W, 36N at a two-year time scale (-736 days), and the strongest negative correlation (-0.327) occurs at 95W, 42N at an approximate 6-month time scale (-192 days). AIRS leads PPT at these scales. AIRS and NDVI lagged correlations exhibit the greatest positive correlation (0.320) at 97.5W, 42N and an approximate annual scale (-400 days). The greatest negative correlation (-0.309) at 90W, 32N is indicative that AIRS lags NDVI at the seasonal to annual scale (224 days).

When examining lagged correlations between NDVI and PPT, the greatest positive correlation (0.506) is located at 97.5W, 32N where PPT lags NDVI at the 16-day (-16 days) scale (Figure 5.7). NDVI lags PPT at the annual scale (304 days) at 97.5W, 34N where the greatest negative correlation (-0.394) across the region is found. These

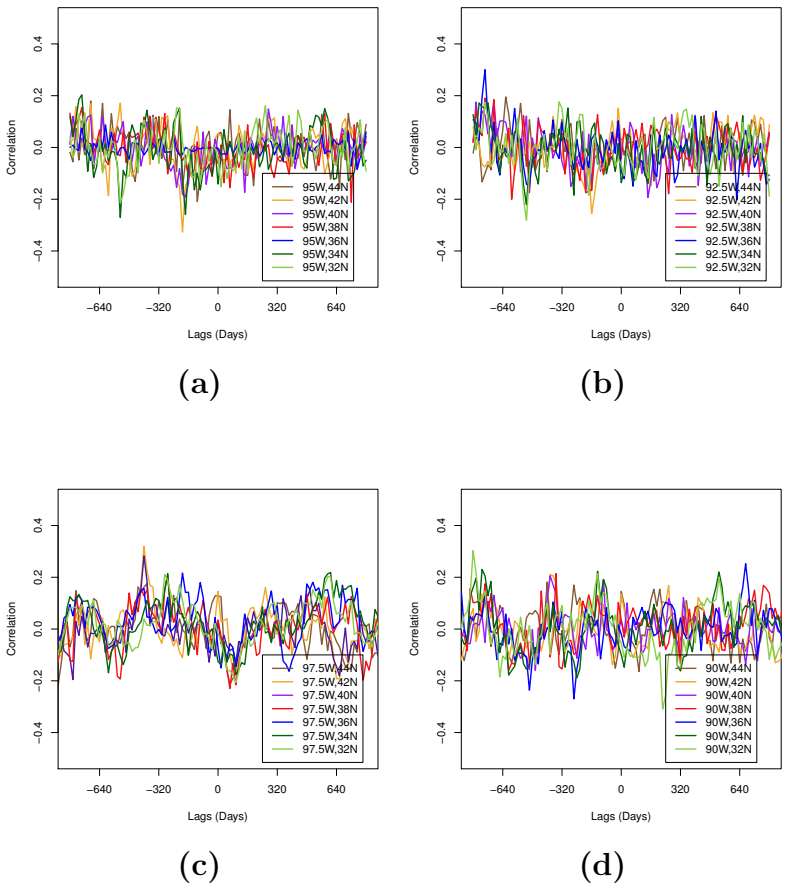

Figure 5.6 Lagged correlations of original AIRS time series with PPT at longitudes of (a) 95W and (b) 92.5W. Lagged correlations of original AIRS time series with NDVI at longitudes of (c) 97.5W and (d) 90W.

relationships can be seen in Figure 5.7a. Similar to lagged correlations between AIRS and NDVI, the periodicity of lagged correlations between NDVI and PPT are greater in the west than the east (Figure 5.7b).

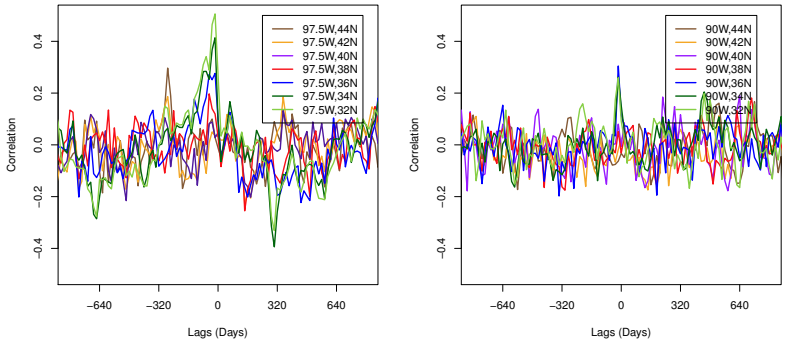

(a) **(b)**

Figure 5.7 Lagged correlations of original PPT and NDVI time series corresponding to longitudes of (a) 97.5W and (b) 90W.

5.2.1 AIRS CO_2 and PPT

To examine how different time scales of PPT influence carbon dynamics, the correlations between wavelet decomposed versions of the PPT time series and the original AIRS time series were examined. The greatest positive correlations across all pixels exist at the 18-month (512 days) and three-year (1024 days) time scales (Figure 5.8. At the 18-month scale, the more northern latitudes exhibit the strongest positive correlations, up to a value of 0.510 at 97.5W, 44N (Figure 5.10b). In contrast, the more southern latitudes show negative correlations up to -0.433 at 90W, 34N and the area where precipitation is greatest. This implies that at the 18-month time scale increased levels of precipitation may correspond with a greater exchange between the ABL and the free troposphere, decreased levels of mid-tropospheric CO_2, and increased photosynthesis in the southeastern part of the region of study. To further

examine this relationship, correlations at the 18-month scale and the mean annual PPT from the original series are plotted. Figure 5.9 shows that areas with stronger negative correlations have higher mean annual PPT supporting the influence of the precipitation gradient across the region.

Another interesting geographic pattern emerges when examining the decomposed PPT signal and the original AIRS CO_2 time series at the three-year scale shown in Figure 5.10c. This pattern shows positive correlations between precipitation and mid-troposphere CO_2 in the eastern longitudes, especially the southeast, where the highest positive correlation (0.643) was computed at 90W, 32N. Positive correlations indicate that increased PPT may correspond with increased CO_2 respiration. In contrast, a region of negative correlations is seen in the plains of Kansas, Oklahoma, and Nebraska where the greatest negative correlation (-0.422) occurs at 97.5W, 38N. This area coincides with semi-arid, agricultural land that relies on irrigation, which can alter soil moisture-precipitation feedbacks and play a role in land-atmosphere interactions. Though the spatial variation at this time scale is worth mentioning, results at longer time scales may be less reliable than shorter time scales (Percival, 1995; Torrence and Compo, 1998).

Relative entropy values calculated from wavelet decomposed versions of the PPT time series compared to the original AIRS time series indicate good agreement between precipitation and mid-tropospheric CO_2 from the seasonal up to the five-year (2048 days) scale across the region of study. Seasonal agreement is especially strong in the central longitudes 97.5W and 95W across all latitudes as shown in Figure 5.11, including pixels 97.5W, 40N (RE=0.286) and 95W, 40N (RE=0.147) that were compared to the EC tower time series in the first part of the study. At the annual scale, very low relative entropy is computed for almost all latitudes at western longitudes 102.5W and 100W where there is less annual PPT (Figure 5.12).

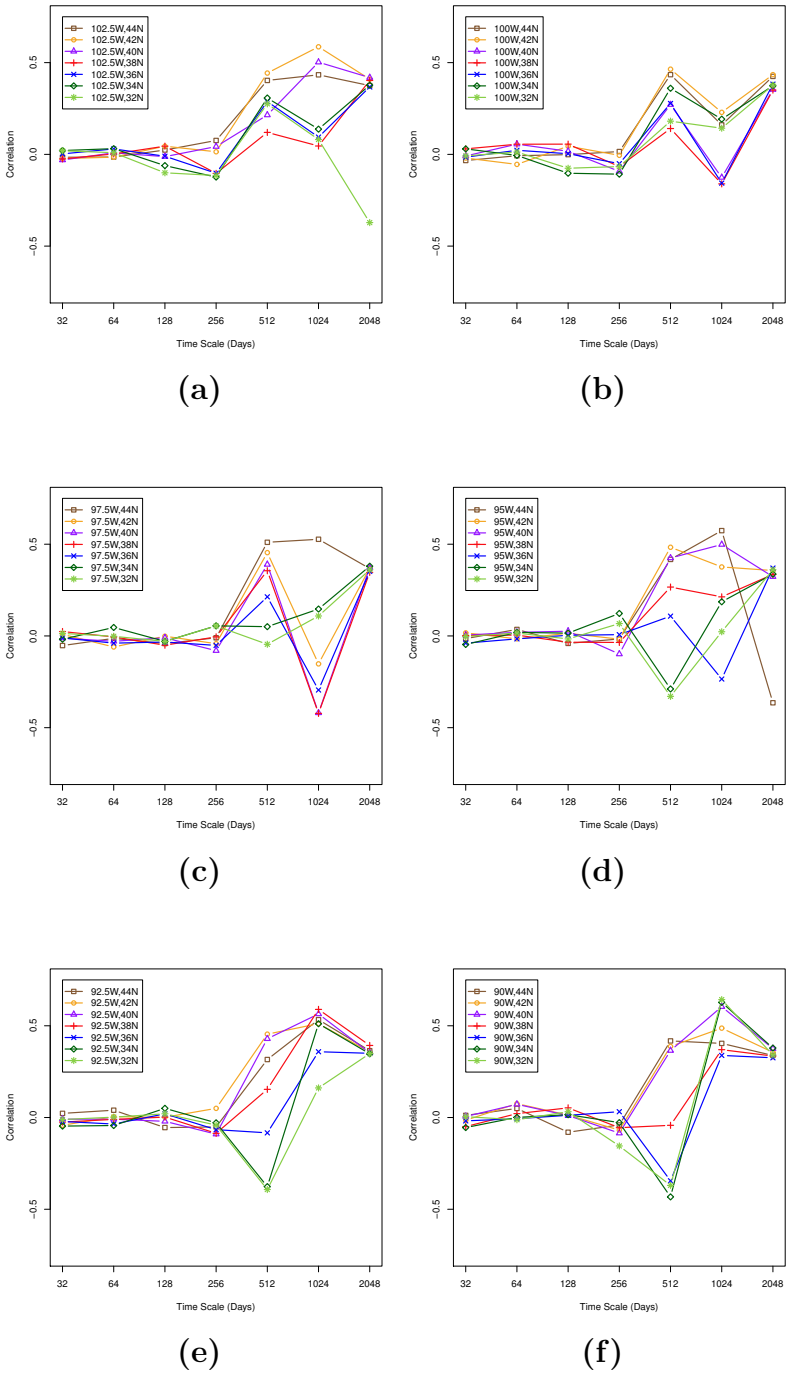

Figure 5.8 Correlations of wavelet decomposed versions of PPT and the original AIRS CO_2 time series across the region of study corresponding to longitudes of (a) 102.5W, (b) 100W (c) 97.5W, (d) 95W, (e) 92.5W, and (f) 90W.

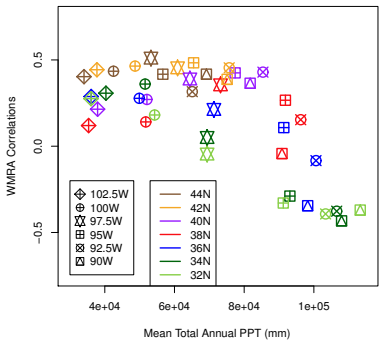

Figure 5.9 Correlations between wavelet decomposed versions of PPT and the original AIRS CO_2 time series at the 18-month (512 day) time scale as compared to mean annual PPT.

5.2.2 AIRS CO_2 and NDVI

To examine how the time scales of vegetation productivity influence atmospheric CO_2 concentrations, wavelet decomposed versions of NDVI were compared to the original AIRS time series. All pixels across the Great Plains region show positive correlations at the 18-month scale (Figure 5.13) suggesting that at this scale high levels of NDVI or vegetation productivity coexist with CO_2 in the mid-troposphere. This could mean one of two things: that higher CO_2 in the mid-troposphere leads to higher vegetation productivity or that higher vegetation productivity corresponds to higher respiration. The answer to which of these scenarios is more likely to play a role may lie in the spatial pattern, where the highest positive correlation (0.490) is located at 102.5W, 44N and the lowest positive correlation (0.140) is found at 90W, 36N. Greater spatial variation exists between mid-tropospheric CO_2 and vegetation phenology at the three-year scale. As illustrated by Figure 5.14c, the highest positive correlation (0.611) at the three-year scale is seen at 100W, 36N, whereas the greatest negative correlation (-0.577) occurs at 102.5W, 32N. Changes associated with land use and land cover over this time period may be responsible.

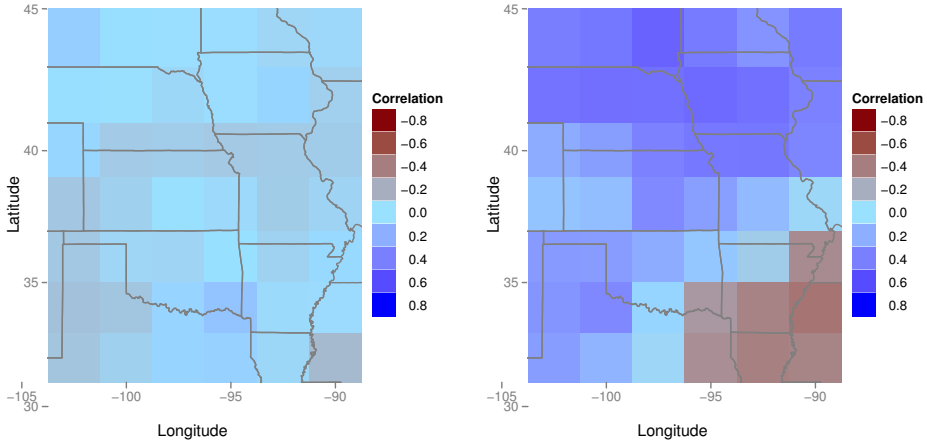

(a) (b)

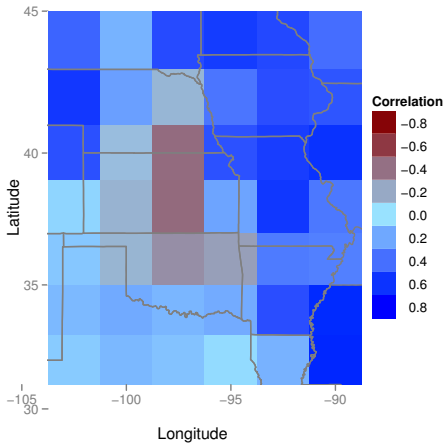

(c)

Figure 5.10 Correlations of wavelet decomposed versions of PPT and the original AIRS CO_2 time series at the (a) annual (256 days), (b) 18-month (512 days), and (c) three-year (1024 days) scale.

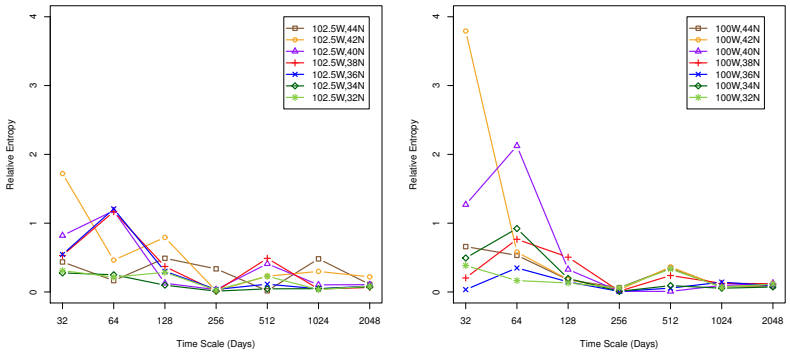

(a)

(b)

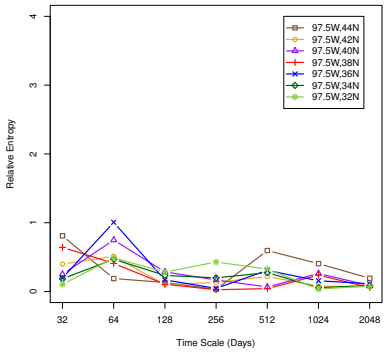

(c)

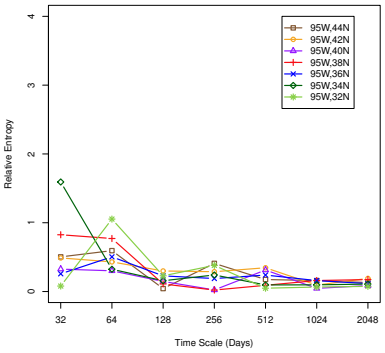

(d)

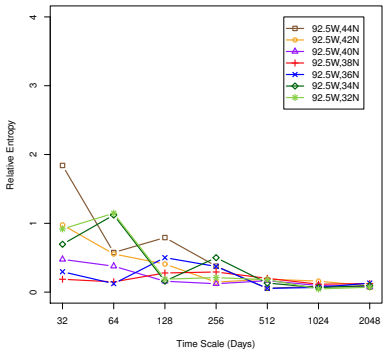

(e)

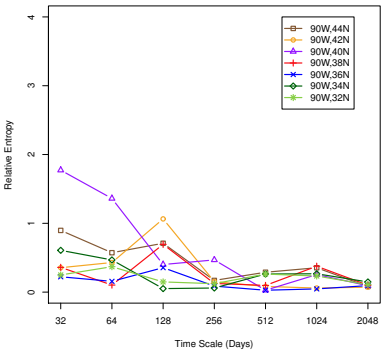

(f)

Figure 5.11 Relative entropy of wavelet decomposed versions of PPT and the original AIRS time series across the region of study corresponding to longitudes of (a) 102.5W, (b) 100W (c) 97.5W, (d) 95W, (e) 92.5W, and (f) 90W.

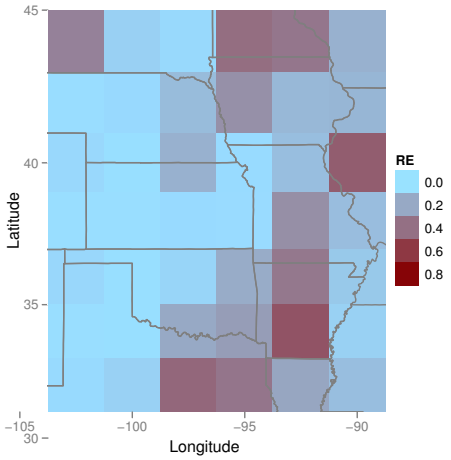

Figure 5.12 Relative entropy of wavelet decomposed versions of PPT and the original AIRS time series at the annual scale.

For the relative entropy of the wavelet decomposed versions of the NDVI time series compared to the original AIRS time series, there continues to be good agreement at the seasonal and longer time scales across the region (Figure 5.15). This is indicative of the strong relationship between vegetation phenology and mid-tropospheric CO_2. Annual scale relative entropies of pixels 97.5W, 40N and 95W, 40N that were compared to the EC tower time series in the first part of the study are 0.069 and 0.094, respectively. These areas also show strong agreement at the three-year scale.

5.2.3 NDVI and PPT

Realizing that vegetation and precipitation are inherently correlated, wavelet multiresolution analysis was applied to PPT and NDVI time series. Not surprisingly, wavelet decomposed versions of the PPT time series compared to the original NDVI time series reveal greatest positive correlations at the annual scale. Moving from west to east, correlations of the more central and southern latitudes approach zero, and correlations become negative in the southeast pixels (Figure 5.16). The highest positive correlation (0.847) is found at 102.5W, 42N and the most negative correlation

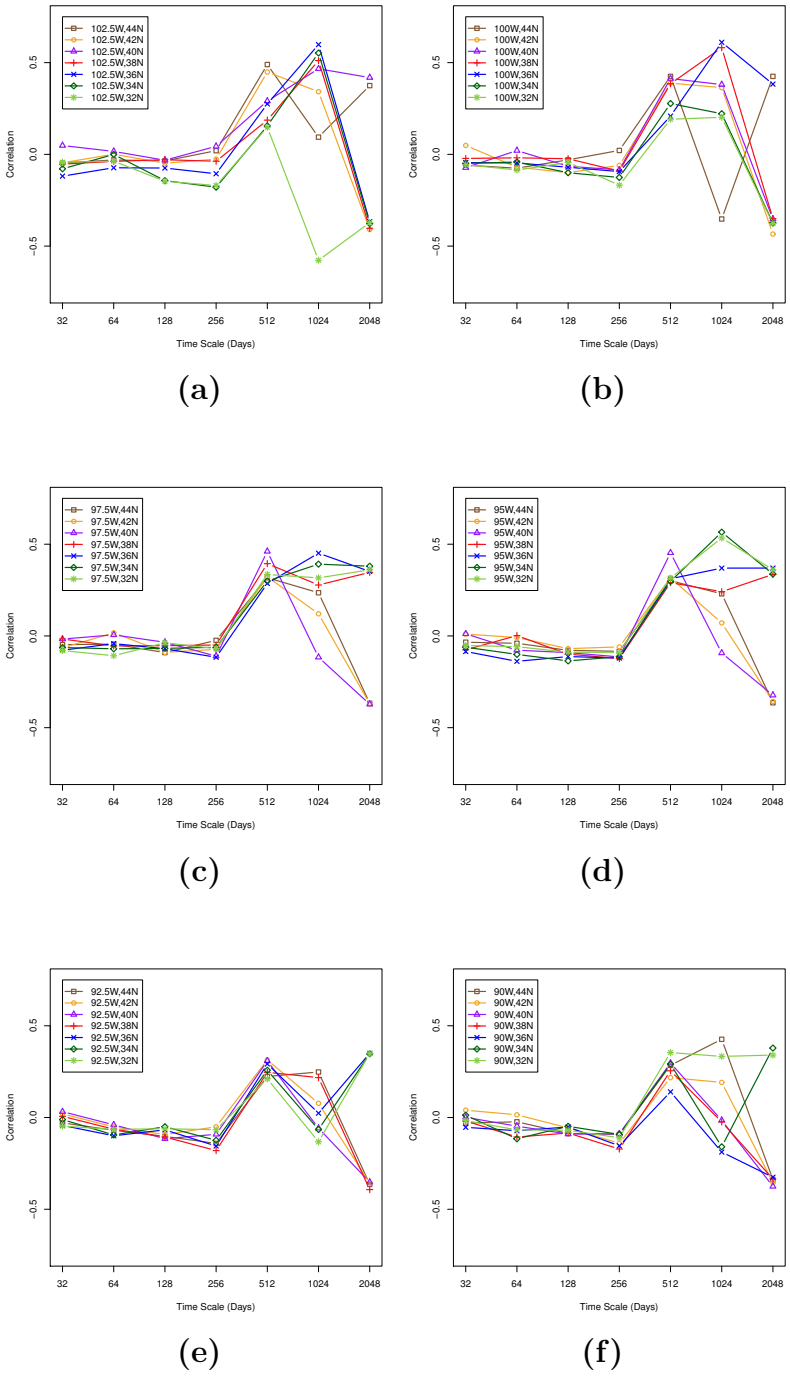

Figure 5.13 Correlations of wavelet decomposed versions of NDVI and the original AIRS CO_2 time series across the region of study corresponding to longitudes of (a) 102.5W, (b) 100W (c) 97.5W, (d) 95W, (e) 92.5W, and (f) 90W.

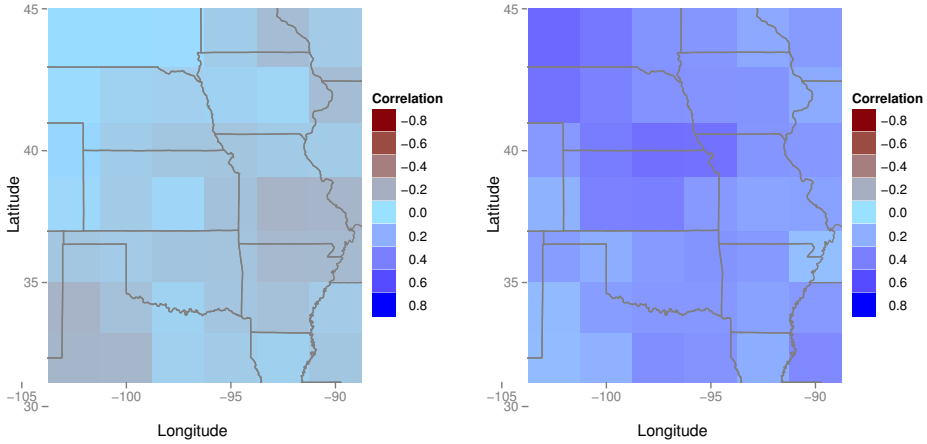

(a) (b)

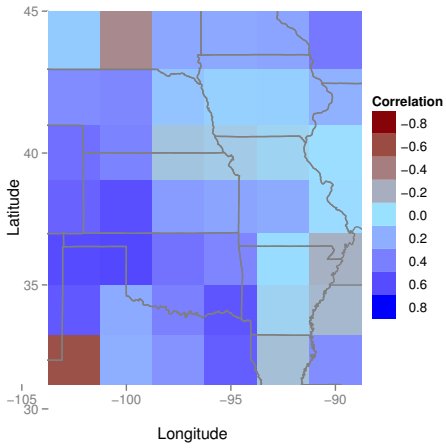

(c)

Figure 5.14 Correlations of wavelet decomposed versions of NDVI and the original AIRS time series at the (a) annual (256 days), (b) 18-month (512 days), and (c) three-year (1024 days) scales.

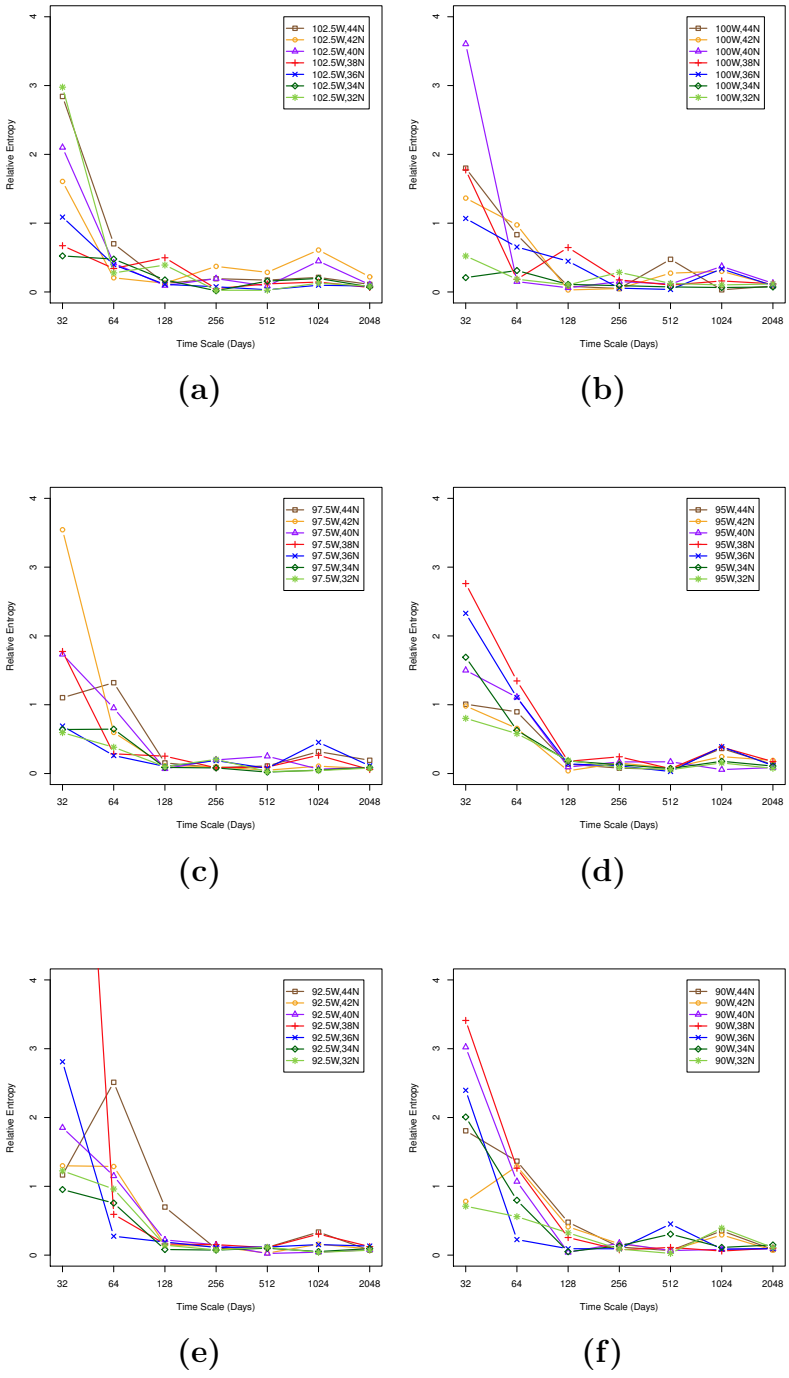

Figure 5.15 Relative entropy of wavelet decomposed versions of NDVI and the original AIRS time series across the region of study corresponding to longitudes of (a) 102.5W, (b) 100W (c) 97.5W, (d) 95W, (e) 92.5W, and (f) 90W.

(-0.249) is seen at 90W, 32N. Similar to Figure 5.10b that illustrates the spatial variation of the PPT gradient on mid-tropospheric CO_2 at the 18-month scale, Figure 5.17a indicates that the influence of this gradient on surface CO_2 processes occurs at the annual scale.

Relative entropy values of the wavelet decomposed versions of PPT compared to the original NDVI time series are low across most pixels at all time scales (Figure 5.18). This is not unexpected as precipitation is a driving factor of vegetation growth. The lowest relative entropy values (between 0.047 and 0.258) for this comparison are found at the annual scale at longitude 100W where mean annual PPT is low (Figure 5.19). Pixels that were compared to the EC tower measurements also have good agreement with RE values of 0.039 at 97.5W, 40N and 0.145 at 95W, 40N.

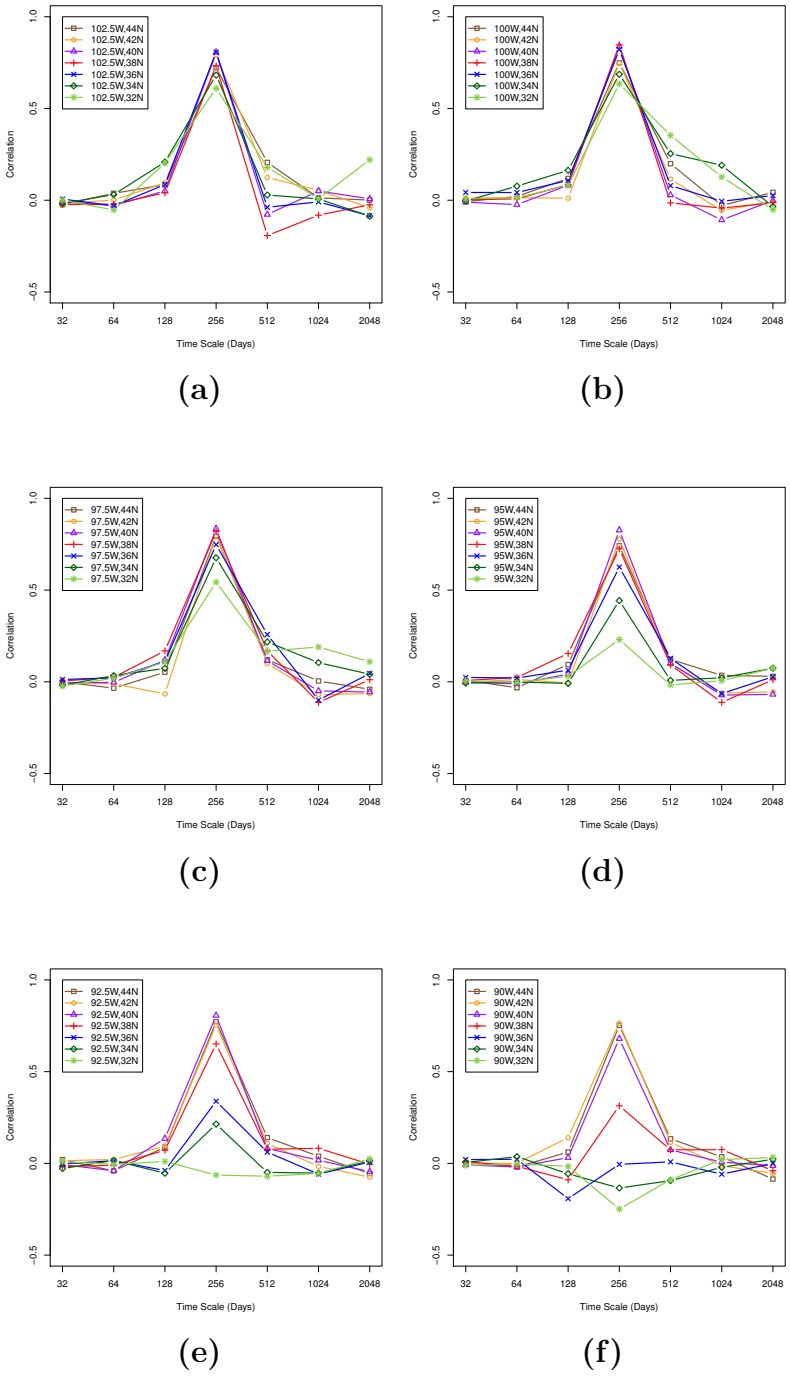

Figure 5.16 Correlations of wavelet decomposed versions of PPT and the original NDVI time series across the region of study corresponding to longitudes of (a) 102.5W, (b) 100W (c) 97.5W, (d) 95W, (e) 92.5W, and (f) 90W.

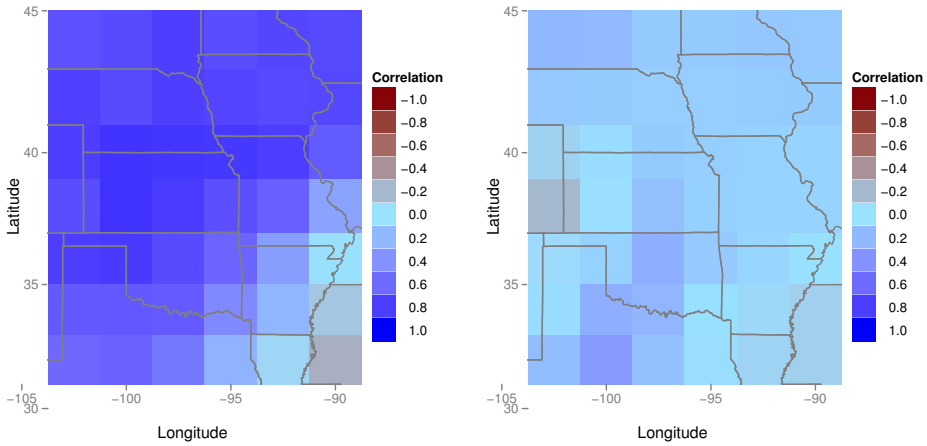

(a) (b)

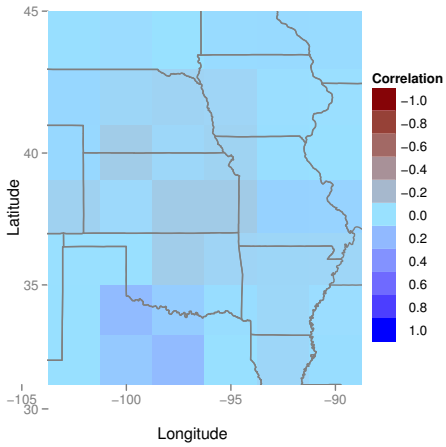

(c)

Figure 5.17 Correlations of wavelet decomposed versions of PPT and the original NDVI time series at the (a) annual (256 days), (b) 18-month (512 days), and (c) three-year (1024 days) scales.

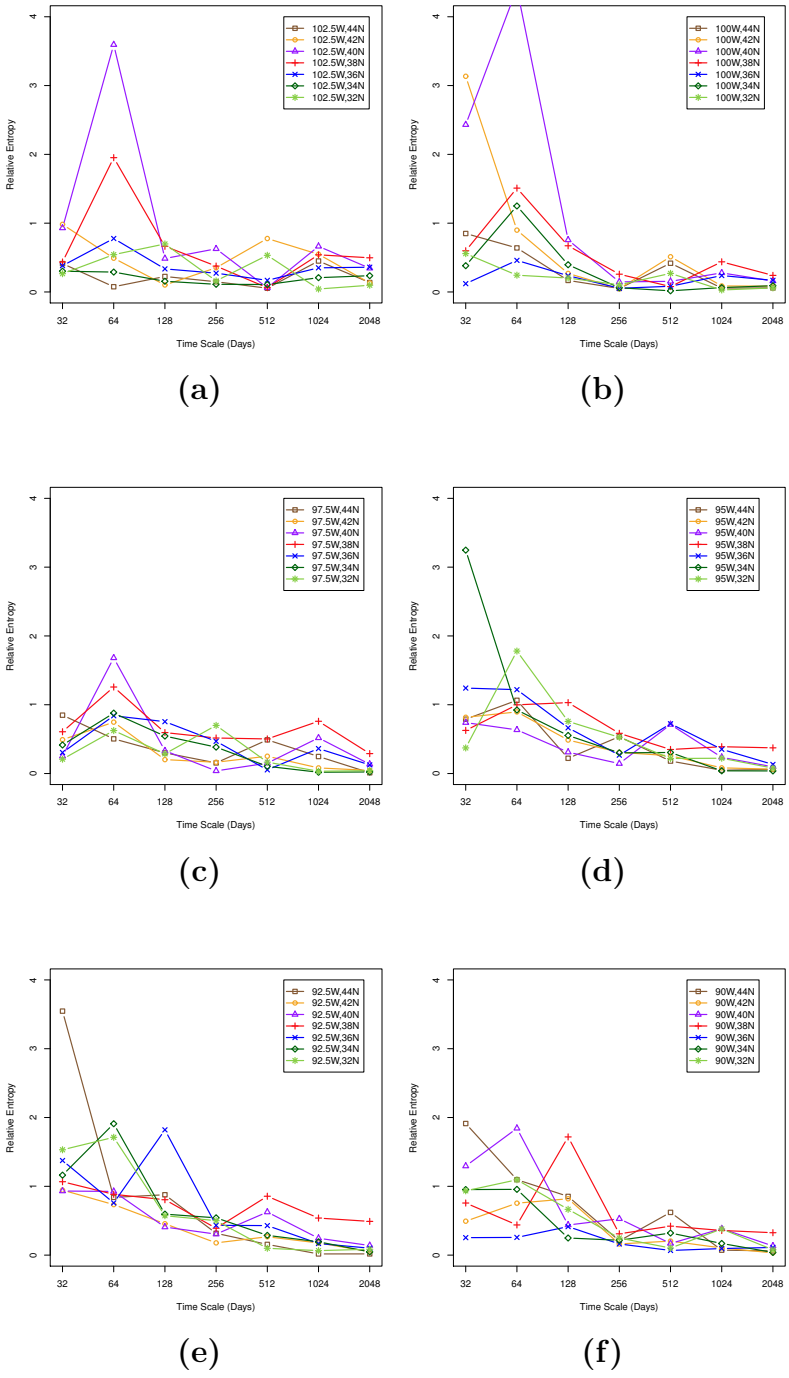

Figure 5.18 Relative entropy of wavelet decomposed versions of PPT and the original NDVI time series across the region of study corresponding to longitudes of (a) 102.5W, (b) 100W (c) 97.5W, (d) 95W, (e) 92.5W, and (f) 90W.

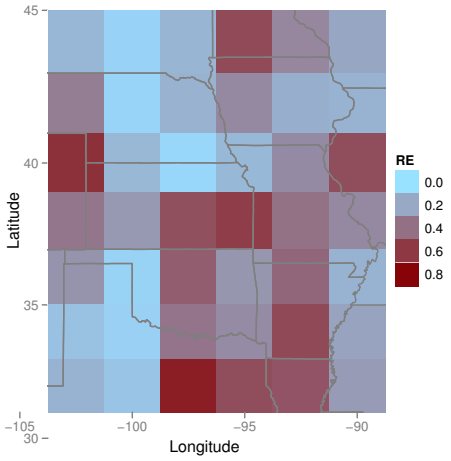

Figure 5.19 Relative entropy of wavelet decomposed versions of PPT and the original NDVI time series at the annual scale.

Chapter 6

Discussion

As previously outlined, ecosystems exhibit complex, nonlinear couplings and feedbacks between biological and atmospheric processes that vary in time and space. Combining results from lagged correlations, wavelet multi-resolution analysis, and the information theory metric of relative entropy, temporal and spatial relationships between surface and mid-troposphere CO_2 and between mid-troposphere CO_2, NDVI, and PPT are evaluated for overarching themes. Correlations from lagged time series and wavelet multi-resolution analysis can provide us with time scales of exchange and contributions between the surface and the mid-troposphere, while the relative entropy metric can reveal how representative one measured variable is of another. Higher correlations in the scales of the wavelet multi-resolution analysis identify the time scale at which there is the greatest contribution of processes and events, corresponding with high or low PPT, NDVI, surface and mid-tropospheric CO_2, from the decomposed time series to the original time series of the other field. As with all correlations, this contribution is not synonymous with causation. Though numerous temporal scales were identified throughout the analyses, discussion will focus on short time scales of days to weeks that might be related to the soil-moisture and precipitation feedback

and synoptic weather, and on longer scales of seasons to years that may relate to climate forcings.

6.1 AIRS and EC Tower Measurements of CO_2 in Northeastern Kansas

When examining the surface and mid-tropospheric CO_2 concentrations, it can be seen that information related to this variable flow both to and from the land surface (Entekhabi et al., 1996; Ruddell and Kumar, 2009a). Still, a simple plot of the original AIRS and EC time series shows that the global signal of CO_2 concentrations in the mid-troposphere exhibits less amplitude or variation on daily to annual scales than surface concentrations (Figure 5.1). This finding is supported by Maddy et al. (2008) and can be explained by the different processes governing the diurnal variability of CO_2 at the surface versus those operating between the ABL and the free troposphere to influence concentrations in the mid-troposphere (Casso-Torralba et al., 2008; Li et al., 2010).

Based on the wavelet multi-resolution analysis and relative entropy metric, assessment of EC tower measurements and AIRS CO_2 observations indicate that land cover as well as topography may play a role in mid-tropospheric concentrations (Nippert et al., in press). Recall that each site has a different land cover type that influences local carbon dynamics and surface fluxes. KFS is located near Lawrence, KS, in an upland tallgrass prairie and deciduous forest ecotone dominated by C_3 grasses and experiencing woody encroachment. This site is burned approximately every five years. KZU is located at the Konza Prairie Biological Reserve in an upland native tallgrass prairie dominated by perennial C_4 grasses, burned annually, and left ungrazed. K4B is the lowland Konza site characterized by a mix of C_3 forbs and C_4 grasses, and burned

every four years.

According to a study conducted on the Konza Prairie by Lett et al. (2004), carbon storage in aboveground biomass greatly increases with shrub encroachment. Shrub islands of *Cornus drummondii* were found to sequester more than nine times the amount of carbon aboveground compared to open grasslands. A shift in plant biomass from belowground in grasslands to aboveground in areas of woody encroachment may cause short-term carbon sinks, though they are more vulnerable to fire and sequester less carbon as woody plants mature. In a complementary Konza Prairie study, annual soil CO_2 flux diminished by 16% as grasslands shifted to shrublands (McCarron et al., 2003).

Juniperus virginiana L. or eastern redcedar is another invasive species of native grasslands in the Great Plains that has been shown to alter ecosystem processes by increasing aboveground NPP, litter, and accrual of organic carbon in litter and soil, while decreasing soil respiration (McKinley and Blair, 2008). Trees also alter soil temperature and microclimate by changing surface albedo. Although it is not known whether sites KFS and K4B are experiencing encroachment of *Cornus drummondii* or *Juniperus virginiana* L., the encroachment of the latter would mean a change from C_4 grasses to C_3 coniferous trees. Analyses of C_3 and C_4 plants within a C_3-C_4 mixed grassland on the Konza Prairie have shown that C_3 plants with greater rooting biomass can be more drought tolerant and continue to photosynthesize beyond C_4 grasses that are drought stressed (Lai et al., 2003). During growing seasons with well-watered conditions, C_4 vegetation contributes approximately 68% to NEE in early spring and up to 100% in late summer (Lai et al., 2003).

Though correlation coefficients are weak for lagged EC and AIRS time series, results indicate that decreases/increases in mid-tropospheric CO_2 concentrations lag increases/decreases in surface concentrations on a seasonal scale, especially over grass-

lands experiencing woody encroachment like sites KFS and K4B. This means that increased respiration rates from soils and increased leaf litter in the winter season may be followed by increased drawdown from encroaching trees and shrubs that green up in the spring season, leading to decreased levels of mid-tropospheric CO_2.

Correlations from the wavelet multi-resolution analysis show the strongest relationships between KFS, KZU, and K4B concentrations and AIRS measurements, and between mid-tropospheric concentrations and KFS, KZU, and K4B measurements, at a time scale of 18 months. The more significant correlations for KZU at this time scale are most likely related to greater soil and biomass respiration found in annually burned grasslands, especially in years of high precipitation, as compared to the sites experiencing woody encroachment (Bremer and Ham, 2010). In addition, Ham et al. (1995) have shown that 85% of respiration in a tallgrass prairie plot, such as KZU, can be attributed to soil respiration.

High/low mid-troposphere CO_2 was associated with high/low surface CO_2 concentrations at both the seasonal and 18-month scale for sites KFS and KZU. KZU also showed a significant positive correlation at the 16-day scale, which may be explained by greater responses of soil respiration to precipitation in grasslands, and soil moisture feedback to synoptic weather patterns (Jones and Brunsell, 2009). K4B behaves as a sink with negative correlations at the 2-month and annual scales.

Results from the relative entropy metric can tell us at which time scales and how well surface measurements correspond with the global signal of CO_2 in the mid-troposphere and vice versa. Mid-tropospheric CO_2 concentrations are well represented by EC tower measurements at the KFS site at all but the four-day time scale, by EC measurements at the KZU site at the 16-day to 2-month scales, and by EC measurements at K4B at the seasonal to annual scales. On the other hand, results show that AIRS measurements may be representative of CO_2 concentrations at the

KFS site at the four-day scale, at the KZU site at 1- and 2-month scales, and at the K4B site at the four-day scale up to the seasonal scale.

The heterogeneity and land cover type at the KFS site is perhaps most characteristic of land cover throughout the region. For this reason, it is not surprising that EC tower measurements at KFS agree with mid-tropospheric concentrations at almost all time scales, nor that AIRS can represent what is happening at the local scale given a time lag as small as four days. K4B, a site that is also experiencing woody encroachment only agrees with mid-tropospheric concentrations at the seasonal to annual scales, while it can be represented by AIRS also at the four-day scale. The relationship between KZU and AIRS remains consistent, with KZU capable of representing mid-tropospheric variation on a 16-day to 2-month scale and AIRS agreeing with surface measurements on a 1- to 2-month scale.

6.2 AIRS CO_2, MODIS NDVI, and PPT in the Great Plains

PPT and mid-tropospheric CO_2 are both climate forcings acting on vegetation at different temporal and spatial scales. Vegetation responses to PPT and CO_2 can be examined through NDVI. Identifying time scales of interactions and agreement between these variables, through wavelet multi-resolution analysis and the information theory metric of relative entropy, may provide future researchers with a starting point for further examination of the influence of the global rise of CO_2 on ecosystem processes. Although lagged correlations may reveal geographic trends, temporal trends across the region of study vary widely. Therefore, focus will remain on correlations and relative entropies of wavelet decomposed versions and original time series.

According to correlation analysis, PPT relates to AIRS mid-tropospheric CO_2

concentrations at the 18-month scale (Figure 5.8). Areas with positive correlations indicate that with higher PPT there is a parallel increase in mid-tropospheric CO_2. As previously mentioned, this may be explained by a positive soil moisture-respiration-precipitation feedback (Jones and Brunsell, 2009).

Negative correlations seen in the southeast, on the other hand, imply that there tends to be a contrasting increase/decrease in PPT or mid-tropospheric CO_2 as these variables decrease/increase. From what is seen in Figure 5.10b, this contribution varies spatially and suggests that areas with higher PPT are associated with lower mid-tropospheric CO_2. The eastern part of the region is also characterized by mixed, broadleaf forests which, depending on stand age, may sequester more carbon. The same spatial pattern is seen in the strong contribution of PPT to NDVI (Figure 5.17a), and to a lesser extent in the contribution of NDVI to PPT, at the annual scale (not shown).

The spatial variation seen at the three-year time scale may be related to agricultural land-use/cover change. This spatial pattern has also been observed during the growing season by the CarbonTracker project and may be attributed to large net uptake in croplands that is not offset by local respiration since biomass is transported elsewhere (Peters et al., 2007). Other possible explanations for the significance of the three-year time scale include the combined influence of crop rotation patterns and the recent trend in corn production to make ethanol. Cultivated acres of corn increased in Kansas, for example, from 1987 to 2007 owing in large part to increased market demand. The price of corn went from $2 a bushel in 2006 to almost $5 a bushel in 2008 (USDA, 2011). A three-year crop rotation system that alternates between corn, wheat, soybeans, or alfalfa is not uncommon in the Midwest.

Ruddell and Kumar (2009a) discussed the information content of variables in synoptic, ABL, and turbulent scales within a Midwestern corn-soybean ecohydrolog-

ical system. They found that the greatest producers of information include gross ecosystem carbon production within the turbulent layer, incoming shortwave radiation within the ABL, and air temperature and vapor pressure deficit at the synoptic scale. While PPT associated with the ABL is considered a moderate sink of information, it plays an important role in transmitting information between weather related synoptic variables and variables involved in processes of photosynthesis and evapotranspiration within the turbulent layer (Ruddell and Kumar, 2009a).

Another explanation for a three-year variation in the spatial relationship between PPT and mid-tropospheric CO_2 may be the effect of ENSO related changes in precipitation and temperature anomalies. Lau and Weng (1995) identified two interannual (2 to 5 year) frequencies in wavelet transforms of the Northern Hemisphere surface temperature time series: a 2.4 year frequency associated with the quasi-biennial oscillation, and a 4.8 year frequency associated with ENSO. Since the region of negative correlation in Figure 5.10c corresponds with one of the hotspots identified by Koster et al. (2004), located in a transition zone between semi-arid and humid climates where precipitation is strongly affected by soil-moisture, periods of drought may decouple processes at synoptic and turbulent scales affecting carbon dynamics in this area (Ruddell and Kumar, 2009a). Logan et al. (2009) have shown that the Standardized Precipitation Index (SPI) has been decreasing in western and northern parts of the Kansas River Basin, corresponding to areas of Eastern Colorado, Northwestern Kansas, and Central Nebraska.

Correlation coefficients of the decomposed versions of NDVI and the original AIRS time series indicate that NDVI is associated the most with mid-tropospheric CO_2 at the 18-month scale. The variation across pixels seen at the three-year scale (Figure 5.14c) may be an indicator of the influence of local land-use/cover change on the global signal of mid-tropospheric CO_2. Recently, it was found that different disturbance

regimes, such as droughts and wildfires, have a big impact on regional NEE across the US, and the temporal variability of these disturbances relative to NEE is yet to be understood (Xiao et al., 2011).

The relationship between PPT and NDVI is found to vary across the PPT gradient of the region and all but the most southeastern pixels exhibit positive correlations. Brunsell (2006) discusses feedback regimes associated with a positive correlation between PPT and NDVI where positive feedbacks result in increases in vegetation, albedo, net radiation, evapotranspiration, and PPT events. Negative correlations are indicative of the occurrence of negative feedbacks where increased vegetation can result in increases in the evaporative fraction and specific humidity, and decreases in sensible heat, the convective boundary layer height, and PPT. Brunsell and Young (2008) also found significant correlations between PPT and NDVI over the Missouri Basin. Using information theory metrics of entropy and mutual information content, they showed that scale-wise correlations between PPT and NDVI increased up to a spatial resolution of 3.2°.

The relative entropy metric indicates that both PPT and NDVI signals agree with AIRS CO_2 on a seasonal scale and longer. This means that PPT and CO_2 involved in processes that drive vegetation growth and senescence agree well with AIRS mid-troposphere CO_2 at the seasonal, annual, and longer scales. In addition, relative entropy of PPT and NDVI show strong agreement across all time scales.

These results agree well with studies that have been conducted to assess the spatial variation of GPP and NEE in the mid-latitudes of the Northern Hemisphere (Beer et al., 2010; Yuan et al., 2009). Yuan et al. (2009) found that mean annual NEE increases with latitude in grasslands and decreases with latitude in deciduous broadleaf and evergreen needleleaf forests. They also found that interannual variability in GPP and respiration in grasslands can be most attributed to interannual

variation in PPT. This result is echoed in the study by Beer et al. (2010) showing that as much as 69% of GPP in temperate grasslands and shrublands is climatically controlled by precipitation.

Given what is known about the soil moisture-precipitation feedback, the temporal and spatial effect of synoptic systems on CO_2 distribution at the surface and in the mid-troposphere, and the influence of PPT on GPP and soil respiration, numerous questions for future research come to mind. Besides the linear rise in global CO_2, what other interannual variations related to ecosystem dynamics can be seen in the global AIRS signal? Can this global signal shape local ecosystems and alter land cover types? Although the answers to these questions are beyond the scope of this study, it is likely that they relate to temporal scales, spatial patterns, and land cover types that have been examined so far.

The comparisons carried out in the initial part of this study make the assumption that the AIRS pixel directly above EC towers best represents local, surface concentrations. Although Parazoo et al. (2008) have shown that surface fluxes and regional scale gradients can be transported by deformation flow and advection related to surface cold fronts, and non-local anomalies can be seen thousands of kilometers downstream, cloudiness usually accompanies these frontal zones. Since AIRS retrievals are selected from cloud-free and cloud-cleared channels, satellite observations may miss these frontal variations as they remain hidden under the clouds. Surface EC tower measurements are much more likely to pick up these non-local surges in CO_2 (Parazoo et al., 2008).

The examination of CO_2 dynamics and transport impeded by cloudy days is not likely to improve even with the additional launch of OCO-2 that will provide regional, 1000-km^2 resolution of near-surface CO_2 measurements every 16-days, but that may still suffer from cloud disturbance with an averaged 18% to 21% of global

observations estimated to be cloud-free (Boesch et al., 2011). As long as AIRS and OCO-2 near-surface measurements remain constrained by cloudy days, dependency on EC towers to measure near-surface fluxes is likely to continue. Continuous surface observations will remain complimentary to satellite measurements, especially in mid-latitudes (Parazoo et al., 2008).

Following the intermediate emissions path in the A1B scenario from the IPCC Special Report on Emissions Scenarios (SRES), Brunsell et al. (2010) predict that Kansas is likely to see warmer temperatures in all seasons with the largest increase on the order of 0.04C yr^{-1} in summer and fall. At the same time, precipitation is likely to decrease in summer and fall, key times affecting agricultural yields and ecosystem respiration, which along with the increase in temperatures will result in a greater water deficit throughout the growing season. The intensity of extreme weather events is also increasing (IPCC, 2007). Flooding and drought events are of particular concern to the agricultural sector across the Great Plains and could have grave repercussions for food availability and prices worldwide.

Future research should also consider the influence of irrigation from the High Plains Aquifer on the regional carbon cycle. As has been shown, irrigation can alter local evapotranspiration and regional precipitation by increasing atmospheric moisture and cooling (Brunsell et al., 2010; Schickedanz, 1976). Another possible repercussion of aquifer mining in the region is the potential influence of water table depth on interannual variability of NEE as hypothesized by Desai (2010).

Chapter 7

Conclusions

Retrieval of CO_2 concentrations in the mid-troposphere by NASA's Atmospheric Infrared Sounder (AIRS) have allowed for examination of the rising global signal of this GHG in relation to surface carbon dynamics, vegetation phenology, and precipitation in the Great Plains. This study has used lagged correlations, wavelet multi-resolution analysis, and the information theory metric of relative entropy to assess the correlations and agreements between mid-tropospheric and surface CO_2 concentrations in Northeastern Kansas. In addition, these methods have been applied to assess the regional relationships between mid-tropospheric CO_2 concentrations, precipitation, and vegetation phenology across the Great Plains.

Results show that surface CO_2 measurements at sites KFS, KZU, and K4B from 2007-2010, and regional PPT and NDVI from 2002 to 2010 correlate well with mid-tropospheric CO_2 at the 18-month time scale. AIRS mid-tropospheric CO_2 observations agree with KFS and K4B at the four-day scale, KZU at the one-month scale, and with PPT and NDVI at seasonal and longer scales. Spatial patterns seen at the 18-month scale for PPT and AIRS are reflective of the influence of PPT on NDVI at the annual scale. Interesting patterns of negative and positive correlations emerge at

the three-year scale and may be indicative of influences of land-use/cover change and intensive agriculture on carbon dynamics, though future research is needed. Continued, long-term and combined surface and mid-tropospheric observations of CO_2 concentrations are essential for an improved understanding of carbon source-sink dynamics in this region.

Bibliography

Arrhenius, S., 1896: On the Influence of Carbonic Acid in the Air Upon the Temperature of the Ground. *Philosophical Magazine and Journal of Science*, **41 (no. 251)**.

Baldocchi, D., 2008: 'Breathing' of the terrestrial biosphere: lessons learned from a global network of carbon dioxide flux measurement systems. *Australian Journal of Botany*, **56 (1)**, 1.

Baldocchi, D., J. Finnigan, K. Wilson, K. T. P. U, and E. Falge, 2000: On Measuring Net Ecosystem Carbon Exchange Over Tall Vegetation on Complex Terrain. *Boundary-Layer Meteorology*, **96**, 257–291.

Baldocchi, D., et al., 2001: FLUXNET: A New Tool to Study the Temporal and Spatial Variability of Ecosystem-Scale Carbon Dioxide, Water Vapor, and Energy Flux Densities. *Bulletin of the American Meteorology Society*, **82 (no. 11)**, 2415–2434.

Baum, K., J. Ham, N. Brunsell, and P. Coyne, 2008: Surface boundary layer of cattle feedlots: Implications for air emissions measurement. *Agricultural and Forest Meteorology*, **148 (11)**, 1882–1893.

Beer, C., et al., 2010: Terrestrial Gross Carbon Dioxide Uptake: Global Distribution and Covariation with Climate. *Science*, **329 (5993)**, 834–838.

Billings, J. S., 1893: *Ventillation and Heating*. The Engineering Record, New York.

Boesch, H., D. Baker, B. Connor, D. Crisp, and C. Miller, 2011: Global Characterization of CO2 Column Retrievals from Shortwave-Infrared Satellite Observations of the Orbiting Carbon Observatory-2 Mission. *Remote Sensing*, **3 (2)**, 270–304.

Bremer, D. J. and J. M. Ham, 2010: Net Carbon Fluxes Over Burned and Unburned Native Tallgrass Prairie. *Rangeland Ecology & Management*, **63 (1)**, 72–81.

Brunsell, N., 2006: Characterization of land-surface precipitation feedback regimes with remote sensing. *Remote Sensing of Environment*, **100 (2)**, 200–211.

Brunsell, N. and R. Gillies, 2003: Scale issues in land–atmosphere interactions: implications for remote sensing of the surface energy balance. *Agricultural and Forest Meteorology*, **117 (3-4)**, 203–221.

Brunsell, N. A., 2010: A multiscale information theory approach to assess spatial–temporal variability of daily precipitation. *Journal of Hydrology*, **385 (1-4)**, 165–172.

Brunsell, N. A., A. R. Jones, T. L. Jackson, and J. J. Feddema, 2010: Seasonal trends in air temperature and precipitation in IPCC AR4 GCM output for Kansas, USA: evaluation and implications. *International Journal of Climatology*, **30 (8)**, 1178–1193.

Brunsell, N. A., S. J. Schymanski, and A. Kleidon, 2011: Quantifying the Thermodynamic Entropy Budget of the Land Surface: Is This Useful? *Earth System Dynamics*, **2 (1)**, 87–103.

Brunsell, N. A. and C. B. Young, 2008: Land surface response to precipitation events using MODIS and NEXRAD data. *International Journal of Remote Sensing*, **29 (7)**, 1965–1982.

Buchwitz, M., O. Schneising, J. P. Burrows, H. Bovensmann, M. Reuter, and J. Notholt, 2007: First Direct Observation of the Atmospheric CO2 Year-to-Year Increase From Space. *Atmospheric Chemistry and Physics*, **7**, 4249–4256.

Callendar, G. S., 1940: Variations of the Amount of Carbon Dioxide in Different Air Currents. *Quarterly Journal of the Royal Meteorological Society*, 395–400.

Casso-Torralba, P., J. Vilà-Guerau de Arellano, F. Bosveld, M. R. Soler, A. Vermeulen, C. Werner, and E. Moors, 2008: Diurnal and vertical variability of the sensible heat and carbon dioxide budgets in the atmospheric surface layer. *Journal of Geophysical Research*, **113 (D12)**.

Chahine, M., C. Barnet, E. T. Olsen, L. Chen, and E. Maddy, 2005: On the determination of atmospheric minor gases by the method of vanishing partial derivatives with application to CO 2. *Geophysical Research Letters*, **32 (22)**.

Chahine, M. T., et al., 2008: Satellite remote sounding of mid-tropospheric CO 2. *Geophysical Research Letters*, **35 (17)**.

Chaumerliac, N. and M. Leriche, 2000: Modeling of scavenging processes in clouds: some remaining questions about the partitioning of gases among gas and liquid phases. *Atmospheric research*.

Cotton, W. R., G. D. Alexander, R. Hertenstein, R. L. Walko, R. L. McAnelly, and M. Nicholls, 1995: Cloud Venting - A Review and Some New Global Annual Estimates. *Earth-Science Reviews*, **39**, 169–206.

Davis, S. J. and K. Caldeira, 2010: Consumption-based accounting of CO2 emissions. *Proceedings of the National Academy of Sciences*, **107 (12)**, 5687–5692.

Desai, A. R., 2010: Climatic and phenological controls on coherent regional interannual variability of carbon dioxide flux in a heterogeneous landscape. *Journal of Geophysical Research*, **115**.

Engelen, R. J. and A. P. McNally, 2004: Estimating atmospheric CO2 from advanced infrared satellite radiances within an operational 4D-Var data assimilation system: Methodology and first results. *Journal of Geophysical Research*, **109 (D19)**.

Entekhabi, D., I. Rodriguez-Iturbe, and F. Castelli, 1996: Mutual Interaction of Soil Moisture State and Atmospheric Processes. *Journal of Hydrology*, **184**, 3–17.

Findell, K. and E. Eltahir, 2003: Atmospheric controls on soil moisture-boundary layer interactions: Three-dimensional wind effects (DOI 10.1029/2001JD001515). *Journal of Geophysical Research*, **108 (8385)**.

Gibert, F., M. Schmidt, J. Cuesta, and P. Ciais, 2007: Retrieval of average co2 fluxes by combining in situ co2 measurements and backscatter lidar information. *Journal of Geophysical Research*, **12 (D10301)**.

Gurney, K. R., D. L. Mendoza, Y. Zhou, M. L. Fischer, C. C. Miller, S. Geethakumar, and S. de la Rue du Can, 2009: High Resolution Fossil Fuel Combustion CO2 Emission Fluxes for the United States. *Environmental Science & Technology*, **43 (14)**, 5535–5541.

Ham, J. M., C. E. Owensby, P. I. Coyne, and D. J. Bremer, 1995: Fluxes of CO2, and Water Vapor From a Prairie Ecosystem Exposed to Ambient and Elevated Atmospheric CO2. *Agricultural and Forest Meteorology*, **77**, 73–93.

Helliker, B. R., J. Berry, A. Betts, and P. Bakwin, 2004: Estimates of net CO2 flux by application of equilibrium boundary layer concepts to CO2 and water vapor measurements from a tall tower. *Journal of Geophysical Research*, **109 (D20)**.

IPCC, 2007: *Climate Change 2007: the Physical Science Basis. Contribution of Working Group I to the Fourth Assessment Report of the Intergovernmental Panel on Climate Change* . Cambridge University Press, Cambridge, United Kingdom and New York, NY, USA.

Jiang, X., M. T. Chahine, E. T. Olsen, L. L. Chen, and Y. L. Yung, 2010: Interannual variability of mid-tropospheric CO2 from Atmospheric Infrared Sounder. *Geophysical Research Letters*, **37 (13)**.

Jones, A. R. and N. A. Brunsell, 2009: Energy Balance Partitioning and Net Radiation Controls on Soil Moisture–Precipitation Feedbacks. *Earth Interactions*, **13 (2)**, 1–25.

Jung, M., M. Reichstein, and A. Bondeau, 2009: Towards Global Empirical Upscaling of FLUXNET Eddy Covariance Observations: Validation of a Model Tree Ensemble Approach Using a Biosphere Model. *Biogeosciences*, **6**, 2001–2013.

Keeling, C. D., 1960: The Concentration and Isotopic Abundances of Carbon Dioxide in the Atmosphere. *Tellus*, **12 (no. 2)**.

Koster, R. D., et al., 2004: Regions of Strong Coupling Between Soil Moisture and Precipitation. *Science*, **305**, 1138–1140.

Kumar, P. and E. Foufoula-Georgiou, 1997: Wavelet Analysis for Geophysical Applications. *Reviews of Geophysics*, **34 (no. 4)**, 385–412.

Lai, C.-T., A. J. Schauer, C. Owensby, J. M. Ham, and J. Ehleringer, 2003: Isotopic Air Sampling in a Tallgrass Prairie to Partition Net Ecosystem CO2 Exchange. *Journal of Geophysical Research*, **108 (no. D18)**, 4566.

Lai, C.-T., A. J. Schauer, C. Owensby, J. M. Ham, B. Helliker, P. P. Tans, and J. R. Ehleringer, 2006: Regional CO2 fluxes inferred from mixing ratio measurements: estimates from flask air samples in central Kansas, USA. *Tellus B*, **58 (5)**, 523–536.

Lambin, E. F. and P. Meyfroidt, 2010: Land use transitions: Socio-ecological feedback versus socio-economic change. *Land Use Policy*, **27 (2)**, 108–118.

Lau, K. and H. Weng, 1995: Climate Signal Detection Using Wavelet Transform: How to make a Time Series Sing. *Bulletin of the American Meteorological Society*, **76 (no. 12)**.

Li, K.-F., B. Tian, D. Waliser, and Y. L. Yung, 2010: Tropical Mid-Tropospheric CO2 variability driven by the Madden-Julian oscillation. *PNAS*, 1–5.

Liu, J., et al., 2007: Complexity of Coupled Human and Natural Systems. *Science*, **317 (5844)**, 1513–1516.

Logan, K. E., N. A. Brunsell, A. R. Jones, and J. J. Feddema, 2009: Assessing spatiotemporal variability of drought in the U.S. central plains. *Journal of Arid Environments*, 1–9.

Maddy, E. S., C. D. Barnet, M. Goldberg, C. Sweeney, and X. Liu, 2008: CO2 retrievals from the Atmospheric Infrared Sounder: Methodology and validation. *Journal of Geophysical Research*, **113 (D11)**.

McCarron, J. K., A. K. Knapp, and J. M. Blair, 2003: Soil C and N Responses to Woody Plant Expansion in a Mesic Grassland. *Plant and Soil*, **257**, 183–192.

McKinley, D. and J. Blair, 2008: Woody Plant Encroachment by Juniperus Virginiana in a Mesic Native Grassland Promotes Rapid Carbon and Nitrogen Accrual. *Ecosystems*, **11 (3)**, 454–468.

Monson, R. K., et al., 2005: Climatic influences on net ecosystem CO2 exchange during the transition from wintertime carbon source to springtime carbon sink in a high-elevation, subalpine forest. *Oecologia*, **146 (1)**, 130–147.

Owensby, C. E., J. M. Ham, and L. M. Auen, 2006: Fluxes of CO2 From Grazed and Ungrazed Tallgrass Prairie. *Rangeland Ecology & Management*, **59 (2)**, 111–127.

Parazoo, N. C., A. S. Denning, S. R. Kawa, K. D. Corbin, R. S. Lokupitiya, and I. T. Baker, 2008: Mechanisms for Synoptic Variations of Atmospheric CO2 In North America, South America and Europe. *Atmospheric Chemistry and Physics*, **8**, 7239–7254.

Percival, D. P., 1995: On Estimation of the Wavelet Variance. *Biometrika*, **82 (no. 3)**, 619–631.

Peters, W., et al., 2005: An ensemble data assimilation system to estimate CO2 surface fluxes from atmospheric trace gas observations. *Journal of Geophysical Research*, **110 (D24)**.

Peters, W., et al., 2007: An atmospheric perspective on North American carbon dioxide exchange: CarbonTracker. *Proceedings of the National Academy of Sciences*, **104 (48)**, 18 925–18 930.

Pielke, R. A., R. Avissar, M. Raupach, A. J. Dolman, X. Zeng, and A. S. Denning, 1998: Interactions Between the Atmosphere and Terrestrial Ecosystems: Influence on Weather and Climate. *Global Change Biology*, **4**, 461–475.

Potts, D. L., T. E. Huxman, R. L. Scott, D. G. Williams, and D. C. Goodrich, 2006: The sensitivity of ecosystem carbon exchange to seasonal precipitation and woody plant encroachment. *Oecologia*, **150 (3)**, 453–463.

Reichstein, M., et al., 2003: Modeling temporal and large-scale spatial variability of soil respiration from soil water availability, temperature and vegetation productivity indices. *Global Biogeochemical Cycles*, **17 (4)**.

Reichstein, M., et al., 2005: On the separation of net ecosystem exchange into assimilation and ecosystem respiration: review and improved algorithm. *Global Change Biology*, **11 (9)**, 1424–1439.

Riley, W. J., S. C. Biraud, M. S. Torn, M. L. Fischer, D. P. Billesbach, and J. A. Berry, 2009: Regional CO 2and latent heat surface fluxes in the Southern Great Plains: Measurements, modeling, and scaling. *Journal of Geophysical Research*, **114 (G4)**.

Ruddell, B. L. and P. Kumar, 2009a: Ecohydrologic process networks: 1. Identification. *Water Resources Research*, **45 (3)**.

Ruddell, B. L. and P. Kumar, 2009b: Ecohydrologic process networks: 2. Analysis and characterization. *Water Resources Research*, **45 (3)**.

Schickedanz, P. T., 1976: The Effect of Irrigation on Precipitation in the Great Plains. Tech. rep., Illinois State Water Survey at the University of Illinois.

Schotanus, P., F. T. M. Niewstadt, and H. A. de de Bruin, 1983: Temperature Measurement with a Sonic Anemometer and Its Application to Heat and Moisture Fluxes. *Boundary-Layer Meteorology*, **26**, 81–93.

Schulze, E. D., 2006: Biological Control of the Terrestrial Carbon Sink. *Biogeosciences*, **3**, 147–166.

Scott, R. L., T. E. Huxman, D. G. Williams, and D. C. Goodrich, 2006: Ecohydrological impacts of woody-plant encroachment: seasonal patterns of water and carbon dioxide exchange within a semiarid riparian environment. *Global Change Biology*, **12 (2)**, 311–324.

Stoy, P. C., et al., 2009: Biosphere-Atmosphere Exchange of CO2 In Relation to Climate: a Cross-Biome Analysis Across Multiple Time Scales. *Biogeosciences*, **6**, 2297–2312.

Styles, J., et al., 2002: Soil and canopy CO2, 13CO2, H2O and sensible heat flux partitions in a forest canopy inferred from concentration measurements. *Tellus B*, **54 (5)**, 655–676.

Tiwari, Y. K., et al., 2006: Comparing CO2 retrieved from Atmospheric Infrared Sounder with model predictions: Implications for constraining surface fluxes and lower-to-upper troposphere transport. *Journal of Geophysical Research*, **111 (D17)**.

Torrence, C. and G. P. Compo, 1998: A Practical Guide to Wavelet Analysis. *Bulletin of the American Meteorological Society*, **79 (No. 1)**, 61–78.

USDA, 2011: Usda national agricultural statistics service. URL http://www.nass.usda.gov/, URL http://www.nass.usda.gov/.

Webb, E., G. Pearman, and R. Leuning, 1980: Correction of Flux for Density Effects Due to Heat and Water Vapour Transfer. *Quarterly Journal of the Royal Meteorological Society*, **106**, 85–100.

Wilczak, J. M., S. P. Oncley, and S. A. Stage, 2001: Sonic Anemometer Tilt Correction Algorithms. *Boundary-Layer Meteorology*, **99**, 127–150.

Willis, B., 1901: Climate and Carbonic Acid. *Popular Science Monthly*.

Xiao, J., et al., 2011: Assessing net ecosystem carbon exchange of U.S. terrestrial ecosystems by integrating eddy covariance flux measurements and satellite observations. *Agricultural and Forest Meteorology*, **151 (1)**, 60–69.

Yuan, W., et al., 2009: Latitudinal Patterns of Magnitude and Interannual Variability in Net Ecosystem Exchange Regulated by Biological and Environmental Variables. *Global Change Biology*, **15**, 2905–2920.

Zhao, M. and S. W. Running, 2010: Drought-Induced Reduction in Global Terrestrial Net Primary Production from 2000 Through 2009. *Science*, **329 (5994)**, 940–943.